Supporting Information

Stereoselective Primary and Secondary Nucleation Events in Multicomponent Seeded Supramolecular Polymerization

Souvik Sarkar,[a] Aritra Sarkar,[a] Arka Som,[a] Sarit S. Agasti,[a] and Subi J. George[a,]*

[a] New Chemistry Unit and School of Advanced Materials (SAMat), Jawaharlal Nehru Centre for Advanced Scientific Research (JNCASR), Jakkur, Bangalore, 560064, India.

Table of Contents

1.1 General Methods

NMR Measurements: ^{1}H spectra were recorded on a BRUKER AVANCE-400 Fourier transformation spectrometer with 400 MHz. ^{13}C spectra were recorded on a BRUKER AVANCE-400 or JEOL-600 Fourier transformation spectrometer with 100 MHz or 125 MHz respectively. The spectra are calibrated with respect to the residual solvent peaks. The chemical shifts are reported in parts per million (ppm) with respect to TMS. Short notations used are, s for singlet, d for doublet, t for triplet, q for quartet and m for multiplet.

High Resolution Mass Spectrometry (HR-MS): HR-MS was carried out using Agilent Technologies 6538 UHD Accurate Mass Q-TOF-LC/MS.

Optical Measurements: Circular Dichroism (CD) spectra and temperature-dependent CD spectra were recorded on a Jasco J-815 spectrometer where the sensitivity, time constant and scan rate were chosen appropriately. The temperature-dependent measurements were performed with a CDF-426S/15 Peltier-type temperature controller with a temperature range of 273-380 K and adjustable temperature slope. Electronic absorption spectra were recorded on Jasco V-750 UV-Visible Spectrophotometer equipped with a peltier. Fluorescence measurements were carried out on a Jasco FP-8500 spectrofluorometer equipped with a peltier.

Fluorescence lifetime measurements: Time-resolved decay experiments were recorded on a Horiba Delta Flex Time-Correlated Single Photon Counting (TCSPC) instrument. A 442 nm nano-LED and 532 nm nano-LED with a pulse repetition rate of 1 MHz was used as the light source. The instrument response function (IRF) was collected by using a scatterer (Ludox AS40 colloidal silica, Sigma Aldrich). For both 442 nm LED and 532 nm nano-LED light sources, the instrumental full width at half maximum including detector response was 0.2 ns. The excited state decay of the sample was collected by fixing the emission wavelength. The decay was fitted to appropriate best fit multiexponential decay using IBH software (DAS6).

Dynamic Light Scattering (DLS): DLS measurements were carried out using a Zetasizer ULTRA Malvern employing a 633 nm laser at a back scattering angle of 173º.

Transmission Electron Microscopy (TEM): TEM measurements were performed on a JEOL, JEM 3010 operated at 300 kV. Samples were prepared by placing a drop of solution on carbon coated copper grid followed by drying at room temperature.

Structured Illumination Microscopy (SIM): Optical setup for imaging in Structured Illumination Microscopy (SIM) method: The fluorescence images of supramolecular polymers were acquired using an inverted Zeiss ELYRA PS1 microscope in structured illumination mode. Two lasers channel I - 488 nm (200 mW) (Green channel) and channel II - 561 nm (200 mW) (Red channel) have been used for respective excitation of **(R)/(S)-3** and **(S)-2** fluorophores respectively. 10 % laser power from the objective top was used for structured illumination imaging. Imaging was performed using a Zeiss oil–immersion objective (Plan–apochromat 63x/1.40 Oil DIC M27, numerical aperture (NA) 1.40 oil). Fluorescence light was spectrally filtered with emission filters for channel I - MBS–488+EF BP 495–575/LP 750 for laser line 488 nm (channel I) and for channel II - MBS– 561+EF BP 570–650/LP 750 for laser line 561 nm (channel II) and imaged using a PCO edge sCMOS camera (quantum yield > 70 %). Structured illumination images were processed using structured illumination analysis package for Zen software (Zeiss). Additional software has been used for image processing (ImageJ). The channels were merged to investigate the spatial correlation between **(S)-3** and **(R)/(S)-2** emitting fibers.

1.2. Synthetic Schemes and Procedures

Materials: All chemicals are purchased from commercial suppliers and used as such without any further purification. (R), and (S) enantiomers of 1,1′-Binaphthyl-2,2′-diamine were obtained from Aldrich having 99% optical purity and stored at 10 ºC. Analytical thin layer chromatography was carried out on Merck silica gel 60 F- 254. Column chromatography was carried out on silica gel (100-200 mesh). Size Exclusion Chromatography was performed on S-X3 bio beads, with chloroform as the eluting solvent.

Molecules **(R)/(S)-1**,[1] **4**,[2] **8-9**,[1] **10**[3] were synthesized following earlier report. Synthetic schemes followed for the synthesis of (**R)-2**, **(S)-2**, and **(S)-3** are shown in **Scheme S1-S4**.

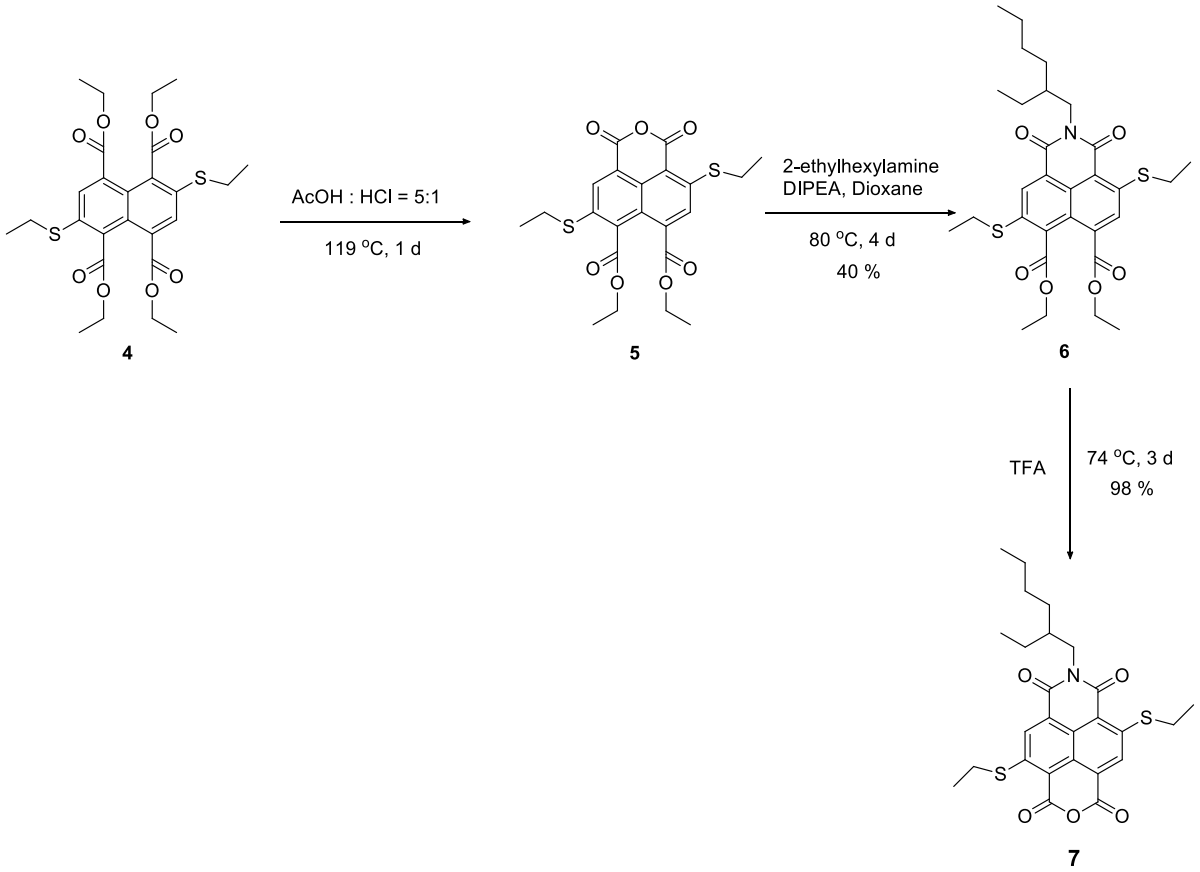

Scheme 1. Synthetic route for the molecule **7**.

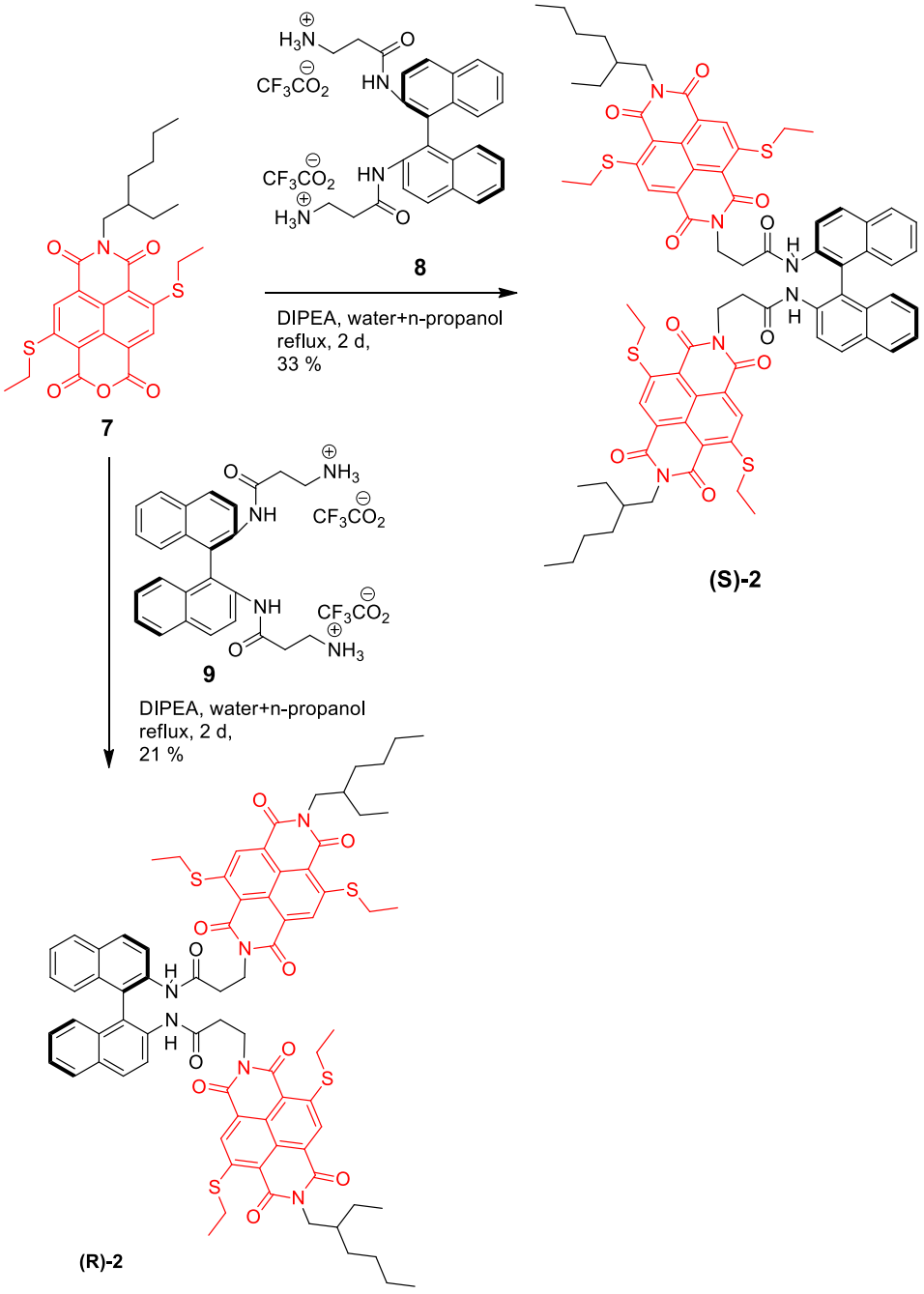

Scheme 2. Synthetic route for the enantiomeric monomers **(R)-2** and (**S**)-**2**.

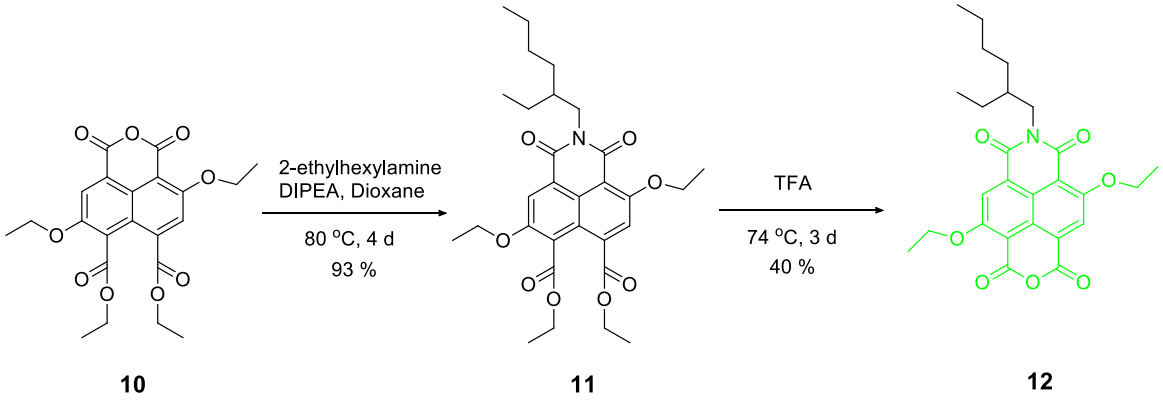

Scheme 3. Synthetic route for the molecule **12.**

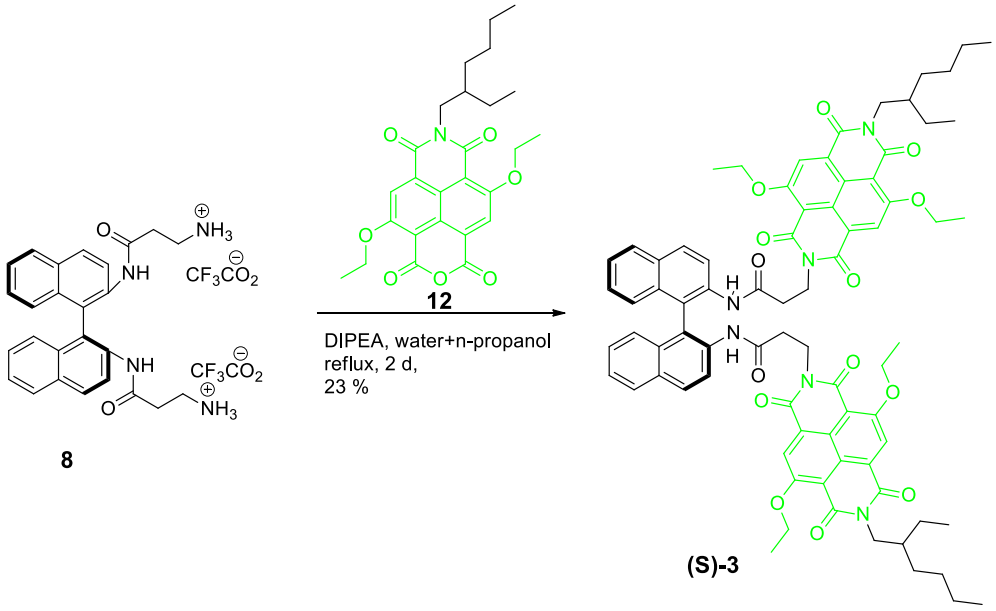

Scheme 4. Synthetic route for the enantiomeric monomer **(S)-3**.

Synthesis of **5.** **1** (760 mg, 1.4 mmol) was taken in a RB flask and 25 mL of acetic acid (AcOH) and 5 mL of conc, HCl were added into it. Then the reaction mixture was refluxed at 119 ºC for 1 day. The completion of the reaction was monitored by TLC with 25/75 (v/v), EtOAc/Hexane as an eluting solvent. After the reaction gets over, the solvent mixture was evaporated under high vacuum. Work-up was done with $CHCl_3$ and water for the removal of excess acetic acid. The organic layer was extracted and evaporated to dryness. The obtained crude product was used without any further purification for the next reaction.

Synthesis of **6.** A mixture of **5** (520 mg, 1.12 mmol), DIPEA (116 mg, 0.09 mmol), and 2-ethylhexylamine (174 mg, 1.3 mmol) were taken in a two-necked RB flask and 50 mL of dioxane was added to it. Then, the reaction mixture was refluxed at 101 ºC for 6 hrs. The progress of the reaction

was monitored by TLC with 25/75 (v/v), EtOAc/Hexane as an eluting solvent. The solvent was evaporated under high vacuum. Work-up was done using 1M HCl and $CHCl_3$ to remove excess of alkyl amine. Then the organic layer was extracted and evaporated to dryness. The purification of the crude product was done using column chromatography (silica gel, 100-200 mesh) with a solvent gradient of 5% EtOAc/Hexane to 20% EtOAc/Hexane to get the pure product **6.** Yield: 40 %. ^{1}H NMR : (400 MHz, $CDCl_3$, ppm) : δ = 8.66 (s, 1H, Ar-H), 7.98 (s, 1H, Ar-H), 4.41 (m, 4H, S-CH_2), 4.18-4.09 (m, 2H, N-CH_2), 3.14 (m, 4H, S-CH_2), 2.04-1.96 (m, 1H, CH), 1.52-0.85 (m, 35H, alkyl H); ^{13}C NMR : (100 MHz, $CDCl_3$, ppm) : δ = 167.4, 166.7, 163.9, 163.0, 148.9, 137.6, 133.6, 133.5, 130.7, 128.2, 127.1, 123.6, 122.6, 117.8, 62.2, 62.0, 44.6, 37.7, 30.7, 29.7, 28.6, 27.9, 26.2, 24.0, 23.1 ,14.0, 14.0, 13.9, 12.8, 10.6; HRMS (ESI) m/z : calculated for $C_{30}H_{39}NO_6S_2$: 573.2219, found for **6**: 574.2287 $[M+H]^+$.

Synthesis of **7**. **6** (260 mg, 0.4 mmol) was taken in a RB flask and 30 mL of trifluoroacetic acid (TFA) was added into it. Then the reaction mixture was refluxed at 75 ºC for 4 days. The completion of the reaction was monitored using TLC with 25/75 (v/v), EtOAc/Hexane as an eluting solvent. After, the reaction gets over; the solvent mixture was evaporated under high vacuum. Purification of the crude product was done using column chromatography (silica gel, 100-200 mesh) with a solvent gradient of 10% EtOAc/Hexane to 30% EtOAc/Hexane to get the pure product **7** as a red powder. Yield: 63 %. ^{1}H NMR : (400 MHz, $CDCl_3$, ppm) : δ = 8.72 (s, 1H, CH-Ar), 8.68 (s, 1H, Ar-H), 4.23-4.13 (m, 2H, N-CH_2), 3.35-3.24 (m, 4H, S-CH_2), 2.01-1.98 (m, 1H, CH), 1.60-0.89 (m, 22H, alkyl CH); ^{13}C NMR : (100 MHz, $CDCl_3$, ppm) : δ = 163.3, 162.3, 159.3, 158.2, 151.0, 149.0, 130.1, 128.7, 127.4, 125.0, 124.7, 120.2, 120.0, 115.0, 44.9, 37.8, 30.6, 28.5, 26.5, 26.3, 24.0, 23.1, 14.0, 12.9, 12.7, 10.5; HRMS (ESI) m/z : calculated for $C_{26}H_{29}NO_5S_2$: 499.1487, found for **7** : 500.1550 $[M+H]^+$.

Synthesis of **(R)-2**. A mixture of **7** (210 mg, 0.42 mmol), **8** (125 mg, 0.19 mmol), and DIPEA (93 mg, 0.7 mmol) were suspended in 30 mL of *n*-propanol and water solvent mixture with a ratio of 2:1 (v/v). Then the reaction mixture was refluxed at 95 ºC for two days. The completion of the reaction was monitored by matrix-assisted laser desorption ionization mass spectrometry (MALDI) and TLC with 20/80 (v/v) EtOAc/Hexane as an eluting solvent. Then the solvent was evaporated under reduced pressure and extracted with DCM and water several times. The organic layer was evaporated to dryness. The purification of the crude product was done using column chromatography with a solvent gradient of 5% EtOAc/Hexane to 15% EtOAc/Hexane (silica gel, 100-200 mesh) to get the pure product, **(R)-2** as the red powder. Yield: 21 %. ^{1}H NMR : (400 MHz, $CDCl_3$, ppm) : δ = 8.62 (d, 2H, J = 8.4 Hz, Ar-H), 8.26 (s, 2H, Ar-H), 8.15 (s, 2H, Ar-H), 8.00 (d, 2H, J = 9.2 Hz, Ar-H), 7.91 (d, 2H, J = 8 Hz, Ar-H), 7.43 (t, 2H, J = 7.4 Hz, Ar-H), 7.29-7.24 (m, 2H, Ar-H), 6.99 (m, 2H, Ar-H), 4.53 (m, 2H, S-CH_2), 4.20-4.10 (m, 6H, S-CH_2), 3.09-2.96 (m, 8H, CH_2), 2.64-2.52 (m, 4H, CH_2), 1.90 (m, 2H, CH), 1.48-0.90 (m, 35H, alkyl H); ^{13}C NMR: (125 MHz, $CDCl_3$, ppm): δ = 170.0, 162.9, 162.6, 162.0, 161.7, 148.6, 148.3, 135.3, 132.5, 131.1, 129.8, 128.1, 127.4, 127.3, 127.1, 125.4, 125.3, 124.1,

124.0, 123.1, 122.6, 121.1, 119.4, 118.3, 117.7, 44.8, 37.7, 36.9, 36.2, 30.9, 30.6, 29.6, 28.6, 26.4, 26.3, 23.9, 23.0, 14.0, 12.5, 10.5. HRMS (ESI) m/z: calculated for $C_{78}H_{80}N_6O_{10}S_4$:1388.4819, found for **(R)-2**: 1411.4640 $[M+Na]^+$.

Synthesis of **(S)-2**. Monomer **(S)-2** was synthesized using similar procedure as used for the synthesis of **(R)-2**. Here, instead of compound **8**, compound **9** was used. Yield: 33 %. ^{1}H NMR : (400 MHz, $CDCl_3$, ppm) : δ = 8.59 (d, 2H, J = 7.2 Hz, CH-Ar), 8.25 (s, 2H, Ar-H), 8.14 (s, 2H, Ar-H), 7.98 (d, 2H, J = 8.8 Hz, Ar-H), 7.89 (d, 2H, J = 8 Hz, Ar-H), 7.40 (t, 2H, J = 7.4 Hz, Ar-H), 7.34-7.21 (m, 4H, Ar-H/NH), 6.98 (m, 2H, Ar-H), 4.48 (m, 2H, S-CH_2), 4.20-4.09 (m, 6H, S-CH_2), 3.08-2.95 (m, 8H, CH_2), 2.61-2.52 (m, 4H, CH_2), 1.89 (m, 2H, CH), 1.49-0.92 (m, 44H, alkyl-H); ^{13}C NMR : (100 MHz, $CDCl_3$, ppm) : δ = 169.8, 163.0, 162.6, 162.1, 161.7, 148. 6, 148.3, 135.4, 132.60, 131.2, 129.9, 128.1, 127.5, 127.4, 127.2, 125.4, 125.3, 124.1, 124.0, 123.2, 122.6, 121.2, 118.4, 117.8, 44.9, 37.7, 36.9, 36.3, 30.7, 29.7, 28.6, 26.4, 26.3, 24.0, 23.1, 14.0, 12.6, 12.6, 10.6; HRMS (ESI) m/z : calculated for $C_{78}H_{80}N_6O_{10}S_4$:1388.4819, found for **(S)-2** : 1389.4873 $[M+H]^+$.

Synthesis of **11**. **10** (410 mg, 0.9 mmol), 2-ethylhexylamine (100 mg, 0.76 mmol), and N,N-diisopropylethylamine (DIPEA) (150 mg, 1.1 mmol) were taken in a 50 mL two necked round bottom (RB) flask. 20 mL dioxane was added to the reaction mixture and then refluxed for an additional day. The progress of the reaction was monitored using thin layer chromatography (TLC) with 25/75 (v/v), ethyl acetate (EtOAc)/Hexane as an eluting solvent. After completion of the reaction, dioxane was evaporated and work-up was done using 1N HCl and dichloromethane (DCM) to remove excess amount of DIPEA. After that, organic layer was extracted and evaporated to dryness. The obtained crude product was used as for the subsequent reaction, without any further purification.

Synthesis of **12**. **11** (150 mg, 0.3 mmol) was taken in a RB flask and 25 mL of trifluoroacetic acid (TFA) was added into it. Then the reaction mixture was refluxed at 74 ºC for 3 days. The completion of the reaction was monitored by TLC with 25/75 (v/v), EtOAc/Hexane as an eluting solvent. After the reaction gets over, the solvent mixture was evaporated under high vacuum. Purification of the crude product was done using column chromatography (silica gel, 100-200 mesh) with a solvent gradient of 10% EtOAc/Hexane to 30% EtOAc/Hexane to get the pure product **12** as a yellow solid. Yield: 41 %. ^{1}H NMR: (400 MHz, $CDCl_3$, ppm): δ = 8.46-8.42 (m, 1H, CH-Ar), 4.52 (m, 4H, O-CH_2), 4.10 (m, 2H, CH_2-ethylhexyl), 1.93 (m, 1H, CH-ethylhexyl), 1.65 (m, 6H, O-CH_3), 1.40-0.86 (m, 16H, CH_2/CH_3-ethylhexyl); ^{13}C NMR : (100 MHz, $CDCl_3$, ppm) : δ = 162.4, 161.3, 161.1, 159.9, 159.8, 155.3, 128.5, 125.7, 123.6, 123.2, 121.5, 119.7, 112.2, 106.7, 66.7, 66.6, 44.7, 37.7, 30.6, 29.7, 28.6, 24.0, 23.0, 14.7, 14.6, 14.0, 10.6; HRMS (ESI) m/z: calculated for $C_{26}H_{29}NO_7$: 467.1944, found for **12**: 468.2027 $[M+H]^+$.

Synthesis of **(S)-3**. A mixture of **12** (140 mg, 0.3 mmol), **8** (80 mg, 0.12 mmol), and DIPEA (180 mg, 1.4 mmol) were suspended in 50 mL of *n*-propanol and water solvent mixture with a ratio of 1:1 (v/v). Then, the reaction mixture was refluxed at 95 ºC for two days. The completion of the reaction was monitored by matrix-assisted laser desorption ionization mass spectrometry (MALDI) and TLC with 30/70 (v/v) EtOAc/Hexane as an eluting solvent. Then the solvent was evaporated under reduced pressure and extracted with DCM and water. The organic layer was evaporated to dryness. The purification of the crude product was done using column chromatography with a solvent gradient of 10% EtOAc/Hexane to 30% EtOAc/Hexane (silica gel, 100-200 mesh), followed by size exclusion chromatography SX-3 to get a pure product as a yellow powder. Yield: 23 %. ^{1}H NMR: (400 MHz, $CDCl_3$, ppm): δ = 8.57 (d, 2H, J = 7.2 Hz, CH-Ar), 8.08 (s, 4H, Ar-H), 7.96 (d, 2H, J = 9.2 Hz, Ar-H), 7.86 (d, 2H, J = 8 Hz, Ar-H), 7.46 (s, 2H, Ar-H), 7.37 (t, 2H, J = 7.4 Hz, Ar-H), 7.21 (m, 2H, Ar-H), 6.97 (d, 2H, J = 7.2 Hz, Ar-H), 4.40-4.33 (m, 10H, O-CH_2/N-CH_2), 4.17-3.99 (m, 6H, CH_2), 2.50 (m, 4H, CH_2), 1.87 (m, 2H, CH), 1.65 (m, 7H, alkyl H), 1.46-0.86 (m, 36H, alkyl H); ^{13}C NMR : (100 MHz, $CDCl_3$, ppm) : δ = 170.0, 162.2, 161.8, 160.6, 160.4, 159.7, 159.5, 135.5, 132.6, 131.2, 129.7, 128.0, 127.1, 126.7, 126.1, 125.4, 125.2, 123.0, 122.7, 121.3, 119.8, 119.1, 110.2, 109.7, 66.2, 66.1, 44.5, 37.7, 36.6, 36.1, 30.7, 28.6, 24.0, 23.1, 14.8, 14.6, 14.1, 10.6; HRMS (ESI) m/z: calculated for $C_{78}H_{80}N_6O_{14}$: 1324.5733, found for **(S)-3** : 1347.5685 $[M+Na]^+$.

1.3. Experimental Procedures:

1.3.1 Protocol of homopolymer sample preparation: Spectroscopic grade solvents were used for performing all the studies. Stock solutions were prepared in tetrachloroethane (TCE) at high concentration and the monomer was injected to methylcyclohexane (MCH) to adjust the final concentration and composition of required choice.

For example: 12.5 μL of 5×10^{-3} M TCE stock of monomer is added to a premixed solution of 62.5 μL of TCE and 2425 μL of methyl cyclohexane (MCH) to prepare the final self-assembling solution of 2.5×10^{-5} M, TCE/MCH, 3/97 (v/v) with a total sample volume of 2500 μL.

1.3.2 Protocol of seed sample preparation: The homopolymeric solutions of (**R)-3** and (**S)-3** were sonicated in a temperature controlled sonicator for about 5 minutes at 20 ºC. Then, the resultant solution is used as seed solution for seeding experiment.

1.3.3 Protocol for homochiral seeding and heterochiral seeding experiments: The self-assembled solution of (**S)-3** (3.5×10^{-5} M, 2500 μL, TCE/MCH, 3/97 (v/v)) was used as seed ((**S)-3$_{Seed}$**). The stock of monomer ((**S)-2$_M$)** for homochiral seeding or (**R)-3$_M$** for heterochiral seeding were prepared at high concentration (10^{-2} M) in TCE to avoid any changes of solvent composition of required choice.

For example: From the prepared monomeric stock, 8.75 μL in TCE was injected to the seed solution and the progress of the supramolecular polymerization was followed by monitoring absorbance

changes at 575 nm. After the completion of the polymerization, an aliquot of seeded solution was given for TEM/SIM for morphological investigation.

1.3.4 Protocol for SIM sample preparation: 20 µL of desired solution was spin-coated on a glass bottom petridish with an r.p.m. of 2000 for 60 s. Then the specimen was used for SIM imaging.

1.3.5 Protocol for TEM grid preparation: 10 µL of desired solution was drop casted on a carbon coated copper grid. After few minutes, ~5 µL of 1% Uranyl acetate was added for negative staining and excess solution wiped off the using Whatman filter paper. Then the grid was kept in a desiccator for about 24 hrs before imaging.

1.3.6 Polydispersity index (PDI) calculation from TEM images: TEM images were recorded for fibres obtained from Seed, homochiral, and heterochiral seeded solution. ~70 fibres were selected from different regions of the grid and analysed using ImageJ software package developed by US. National Institute of Health. The average length (L_n = number average length, and L_w = weight average length) and PDI were calculated using equations (S1-S3), where, N_i is the number of fibres chosen for analysis and L_i is the length of fibres for the sample.

Number average length, $\boldsymbol{L_n} = \sum_{i=1}^{N} \frac{N_i L_i}{N_i}$ (S1)

Weight average length, $\boldsymbol{L_w} = \sum_{i=1}^{N} \frac{N_i L_i^2}{N_i L_i}$ (S2)

Polydispersity index, $\boldsymbol{PDI} = \frac{L_w}{L_n}$ (S3)

1.3.7 Fitting of Heating Curves: Cooperative/Isodesmic fits were performed using MATLAB R2008b software. Though the codes pertain to one component systems, we have extrapolated them to two component systems, and the thermodynamic parameters thus obtained are well within accepted limits.[4]

1.3.8 Mathematical Modelling Information: The growth kinetics of the seeded supramolecular (co)-polymers were fitted using online amylofit software (http://www.amylofit.ch.cam.ac.uk) developed by Knowles and co-workers.[5] In order to identify the dominant self-assembly mechanism during seeding experiments, first the early stage growth kinetics of supramolecular polymerization were analysed, then scaling exponent (γ) and nature of linear fit from double logarithm plot were evaluated, followed by fitting the seeded kinetic profiles using the amylofit software to their respective self-assembly mechanism.

1.3.8.1 Mathematical Model: The mathematical models used to fit the experimental kinetics data were the analytical solutions of the seed-induced various models derived by Knowles and co-workers.[5] For instance, seed-induced nucleation-elongation, seed-induced secondary nucleation, seed-

induced multistep secondary nucleation models were used in this present manuscript, the mathematical models are described as follows:

1.3.8.1.2 Seed induced nucleation-elongation model:

The analytical solution of nucleation-elongation model is:

$$\frac{M}{m_t} = 1 - \frac{m_0}{m_{tot}}\left(\frac{1}{\mu}\cosh\left(sqrt(\frac{n_1}{2}\mu\lambda t + \nu)\right)\right)^{-\frac{2}{n_1}} \quad \text{(S4)}$$

$$\lambda = sqrt(2k_+k_n m_0^{n_1}) \quad \text{(S5)}$$

$$\alpha = sqrt(\frac{k_+ n_1}{k_n m_0^{n_1}} P_0) \quad \text{(S6)}$$

$$\mu = sqrt(1+\alpha^2) \quad \text{(S7)}$$

$$\nu = \log(\alpha+\mu) \quad \text{(S8)}$$

1.3.8.1.3 Seed induced secondary nucleation:

$$\frac{\mathrm{M}}{\mathrm{M}_\infty} = 1 - \left(1 - \frac{M_0}{M_\infty}\right)e^{-k_\infty t}\left(\frac{B_- + C_+ e^{kt}}{B_+ + C_+ e^{kt}} \times \frac{B_+ + C_+}{B_- + C_+}\right)^{\frac{k_\infty}{kk'_\infty}} \quad \text{(S9)}$$

$$k = sqrt(2m_0 k_+ m_0^{n_2} k_2) \quad \text{(S10)}$$

$$\lambda = sqrt(2k_n k_+ m_0^{n_1}) \quad \text{(S11)}$$

$$C_\pm = \frac{k_+ P_0}{k} \pm \frac{k_+ M_0}{2m_0 k_+} \pm \frac{\lambda^2}{2k^2} \quad \text{(S12)}$$

$$k_\infty = sqrt(\left(2k_+ P(0)\right)^2 + \frac{4k_+k_n m_0^{n_1}}{n_1} + \frac{4k_+k_2 m_{tot} m_0^{n_2}}{n_2} + \frac{4k_+k_2 m_0^{n_2+1}}{n_2+1}) \quad \text{(S13)}$$

$$k'_\infty = sqrt(k_\infty^2 - 2C_+C_-k^2) \quad \text{(S14)}$$

$$B_\pm = \frac{k_\infty \pm k'_\infty}{2k} \quad \text{(S15)}$$

1.3.8.1.4 Seed induced multistep secondary nucleation:

$$\frac{\mathrm{M}}{\mathrm{M}_\infty} = 1 - \left(1 - \frac{M_0}{M_\infty}\right)e^{-k_\infty t}\left(\frac{B_- + C_+ e^{kt}}{B_+ + C_+ e^{kt}} \times \frac{B_+ + C_+}{B_- + C_+}\right)^{\frac{k_\infty}{kk'_\infty}} \quad \text{(S16)}$$

$$k = sqrt(2m_0 k_+ \frac{m_0^{n_2} k_2}{1 + m_0^{n_2}/k_M}) \quad \text{(S17)}$$

$$\lambda = sqrt(2k_n k_+ m_0^{n_1}) \quad \text{(S18)}$$

$$C_{\pm} = \frac{k_+ P_0}{k} \pm \frac{k_+ M_0}{2 m_0 k_+} \pm \frac{\lambda^2}{2k^2} \quad \text{(S19)}$$

$$k_\infty = sqrt(\left(2k_+ P(0)\right)^2 - 2A - 4k_+ k_2 m_{tot} K_M \frac{\log[K_M]}{n_2}) \quad \text{(S20)}$$

$$A = -\frac{2k_+ k_n m_0^{n_1}}{n_1} - 2k_+ k_2 m_{tot} K_M \frac{\log[K_M + m_0^{n_2}]}{n_2} - 2k_+ k_2 m_0 K_M \left(\frac{1}{2} F[\frac{1}{n_2}, 1{,}1 + \frac{1}{n_2}, -\frac{m_0^{n_2}}{K_M}\right] - 1) \quad \text{(S21)}$$

$$k'_\infty = sqrt(k_\infty^2 - 2C_+ C_- k^2) \quad \text{(S22)}$$

$$B_{\pm} = \frac{k_\infty \pm k'_\infty}{2k} \quad \text{(S23)}$$

Parameters involved in above equations (S4-S23):

P = Fiber number concentration (number concentration of supramolecular polymer)

M = Fiber mass concentration (mass concentration of supramolecular polymer)

m = Monomer concentration

k_{n1} = rate of primary nucleation

k_{n2} = rate of secondary nucleation

n_1 = reaction order of primary nucleation

n_2 = reaction order of secondary nucleation

K_M = Michaelis constant for secondary nucleation

For fitting the growth kinetics of the seeded supramolecular (co)-polymers using online amylofit software (http://www.amylofit.ch.cam.ac.uk), first we have evaluated the primary and secondary reaction order from double logarithm plot (See main text, Figure 1f and 3g) and set these values as a global constant. For seeding experiment, as fiber number concentration (P) is a required parameter, but experimentally it is very difficult to measure the numbers of fiber used as a seed solution.[5] Instead, the values for P was chosen as arbitrarily (two or three orders of magnitudes smaller than initial aggregate concentration). For example, in seed-induced nucleation-elongation model fitting, it was set as 10^{-7} M: in seed-induced multistep secondary nucleation: 10^{-8} M; seed-induced secondary nucleation: 5×10^{-7} M.

Further, effects of reaction orders on the fitting of seeded kinetics of their respective models were also assessed to justify the goodness fit. We found out that reaction order associated with lowest mean squared error (MSE) was experientially matches with the reaction order (evaluated from double logarithm plot of half-time and monomer concentration).

1.4. Supporting Figures:

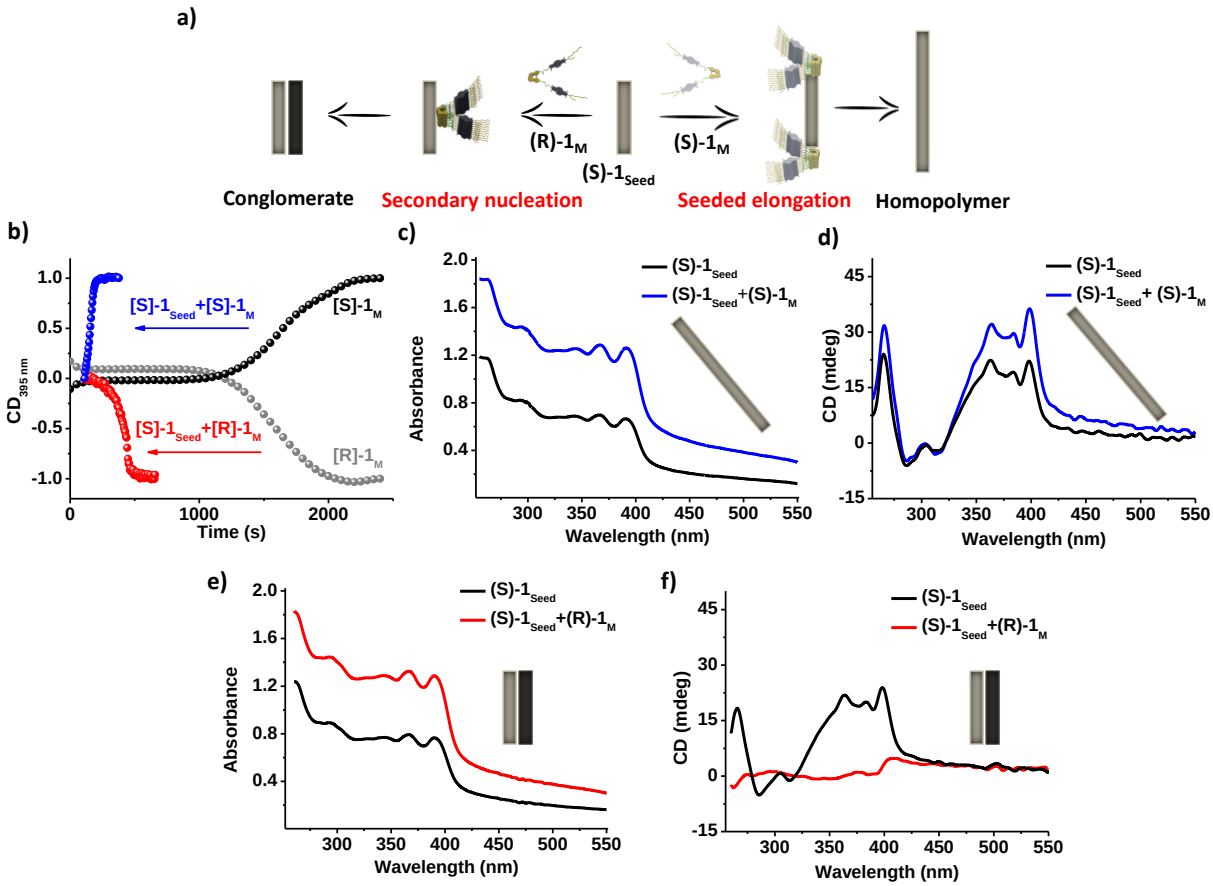

Figure S1. a) Schematic representation of chirality control over primary nucleation-elongation and secondary nucleation process during the seeded supramolecular polymerization process of the enantiomeric monomers of **1**. b) Time-dependent mirror-image CD intensity monitored at 395 nm showing the kinetically controlled growth of **(R)/(S)-1** homopolymers in TCE/MCH, 1/99 (v/v) solvent mixtures (black and grey dotted lines). Time-dependent CD intensity changes for homochiral seeding (blue dotted line) and heterochiral seeding (red dotted line) on introduction of **(S)-1$_M$** and **(R)-1$_M$** monomers, respectively into kinetically grown seeds of **(S)-1$_{Seed}$**. Steady-state c,e) absorption, and d,f) CD spectra of only seed (**(S)-1$_{Seed}$**) and homochiral seeded (**(S)-1$_{Seed}$+(S)-1$_M$**) and heterochiral seeded (**(S)-1$_{Seed}$+(R)-1$_M$**) solutions. (1/99, TCE/MCH (v/v), [**(S)-1$_{Seed}$**] = [**(S)-1$_M$**] = [**(R)-1$_M$**] = 5 × 10^{-5} M, 25 ^{o}C, l = 10 mm)

Note. **(R)/(S)-1** enantiomers show mirror image kinetic profiles during the formation of thermodynamic supramolecular homopolymers from its metastable state, characteristic of a kinetically controlled cooperative supramolecular homopolymerization process. Upon introduction of **(S)-1$_M$** monomers into kinetically grown **(S)-1$_S$** seed, it shows spontaneous growth kinetics indicating seeded nucleation-elongation process (blue line in figure S1b). On the other hand, upon introduction of **(R)-1$_M$** monomers into kinetically grown **(S)-1$_S$** seed, it shows sigmoidal growth kinetics indicating

secondary nucleation to the existing pre-grown seed (red line in figure S1b). It is noteworthy to mention that the CD signal becomes zero for heterochiral seeding experiment with the 1:1 equivalent of seed and monomer ratio due to the formation of a conglomerate. For homochiral seeding study, the optical density and its corresponding CD signal increases for seeded solutions. On the other hand, for the heterochiral seeding study, the optical density of the resultant seeded solution increases and the resultant CD signal reaches to zero.

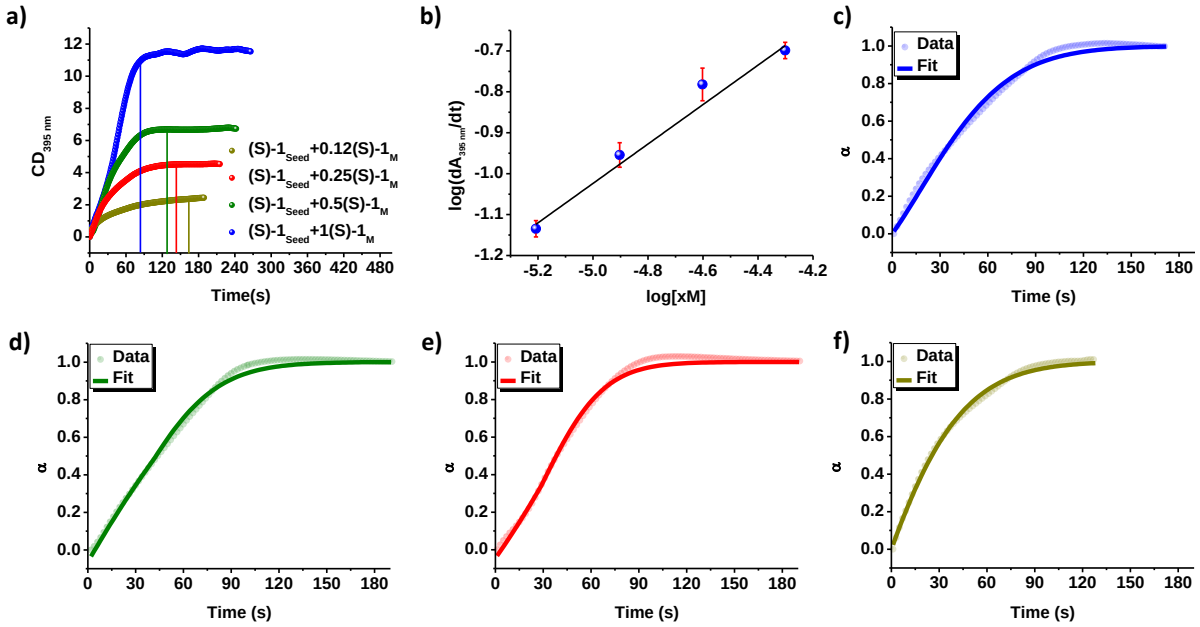

Figure S2. a) Time-dependent CD intensity changes monitored at 395 nm for homochiral seeded supramolecular polymerization using constant **(S)-1$_{Seed}$** concentration (5×10^{-5} M) and varying concentrations of corresponding monomer (6×10^{-6} M to 5×10^{-5} M) indicating a spontaneous growth kinetics, characteristic of seed-induced primary nucleation-elongation process. b) Log-log plot of rate of seeded supramolecular polymerization (calculated from main text, figure 1d) with the monomer concentration, which shows a linear trend with a slope of 0.99 suggesting a seeded chain-growth supramolecular polymerization process. c-f) Fitting of homochiral seeded kinetics (extracted from main text, figure 1d) into seed-induced nucleation-elongation model by using online software http://www.amylofit.ch.cam.ac.uk at constant seed concentration ([**(S)-1$_{Seed}$**] = 5×10^{-5} M) and variable feed monomer ([**(S)-1$_{M}$**] concentration: c) 6×10^{-6} M, d) 1.25×10^{-5} M, e) 2.5×10^{-5} M, and f) 5×10^{-5} M. (α = degree of supramolecular polymerization, 1/99, TCE/MCH (v/v), 25 ºC, 10 mm)

Note: The homochiral seeding of **(S)-1**, indicates that the primary nucleation-elongation dominated seeded supramolecular polymerization mechanism and is a good-fit into seed-induced nucleation-elongation model with a Mean Squared Error (MSE) less than 0.0007 (table S1).[5]

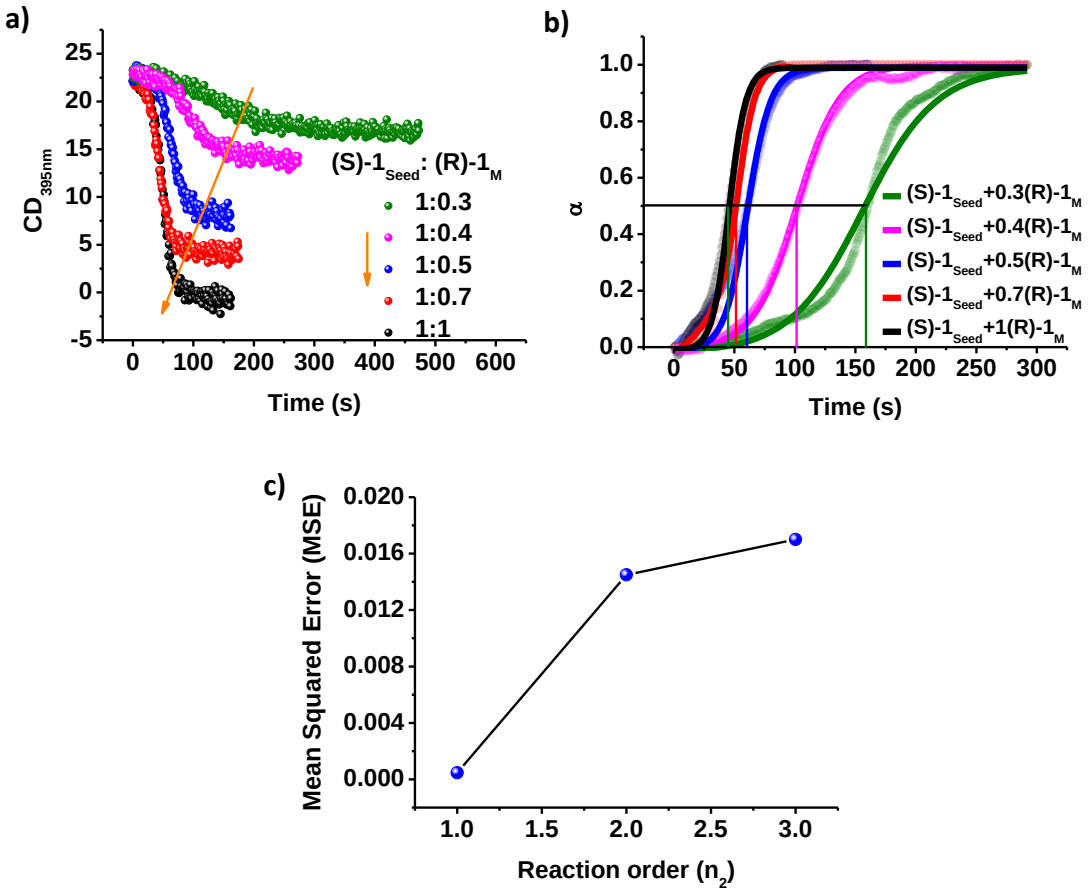

Figure S3. a) Kinetic profiles of heterochiral seeded supramolecular polymerization by monitoring the CD intensity changes at 395 nm at constant **(S)-1$_{Seed}$** concentration (5×10^{-5} M) and varying concentrations of corresponding monomer, **(R)-1$_{M}$** (1.5×10^{-5} M to 5×10^{-5} M). b) Poor fitting of kinetic profiles for concentration-dependent heterochiral seeding in seed-induced secondary nucleation model using online software http://www.amylofit.ch.cam.ac.uk. The solid lines indicate the poor secondary nucleation fit with a mean squared error (MSE) of 0.0018.[5] c) Effect of reaction order (n_2) on the error of fitting with multistep secondary nucleation model (Main text, figure 1e). This indicates with increasing reaction order, the mean squared error (MSE) increases hinting towards poor fitting of the heterochiral seeded kinetics (1/99, TCE/MCH (v/v), 25 ºC, 10 mm)

Note: The concentration-dependent heterochiral seeding studies using **(S)-1$_{Seed}$** as a seed and **(R)-1$_{M}$** as a feed monomer indicates that increasing the monomer equivalent from 0.3 to 1 resulted in the decrease of the half-time (t_{50}) with a sigmoidal nature of the growth kinetics. A poor fit of sigmoidal growth kinetics was obtained by using secondary-nucleation model with a mean squared error (MSE) of 0.0018, but a better fit with lower MSE value of 0.0003 was obtained with a multistep secondary nucleation model (Main Text, figure 1e).[5] The reaction order (n_2) 1 with lowest MSE matches well with experimentally evaluated reaction order from the scaling exponent.

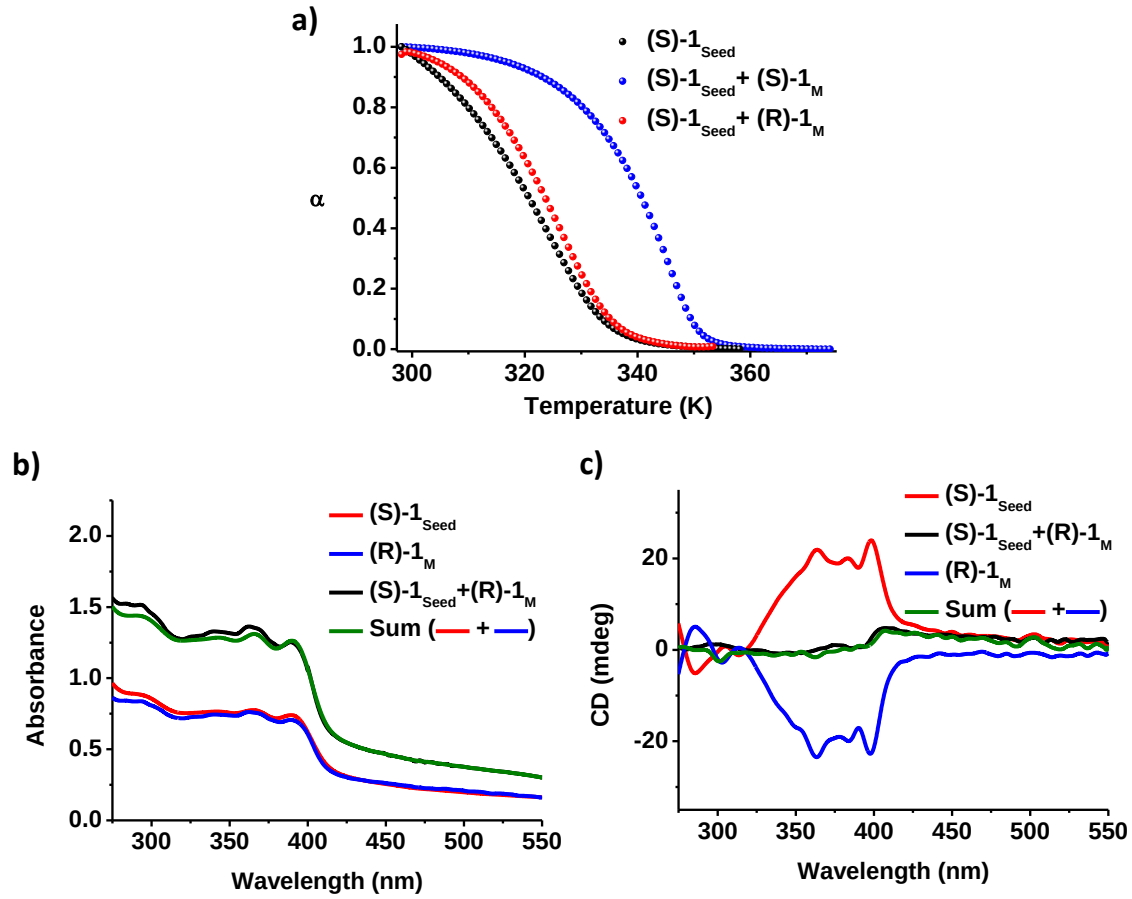

Figure S4. a) Temperature-dependent melting curves monitored at 395 nm absorbance band indicate increased thermal stability for homochiral seeded solution (**(S)-1$_{Seed}$+(S)-1$_M$**) and unaltered thermal stability for heterochiral seeded solution (**(S)-1$_{Seed}$+(R)-1$_M$**) with respect to its **(S)-1** homopolymer. ([**(S)-1$_{Seed}$**] = [**(R)-1$_M$**] = [**(S)-1$_M$**] = 5×10^{-5} M, TCE/MCH, 1/99 (v/v), 10 mm). Spectra analyses after heterochiral-seeding experiments. Plots of b) absorption, and c) CD spectra of heterochiral seeded **(S)-1$_{Seed}$+(R)-1$_M$)** solutions by using **(S)-1$_{Seed}$** as a seed solution and **((R)-1$_M$** as a feed monomer. Absorption, and CD spectrum of the heterochiral seeded solutions **((S)-1$_{Seed}$ + (R)-1$_M$)** is identical to the simple summation (seed+feed monomer) of the homopolymer's spectrum. **([(S)-1$_{Seed}$ = [(R)-1$_M$]** = 5 × 10^{-5} M, TCE/MCH, 1/99 (v/v), l = 10 mm, 25 ºC).

Note: An unambiguous proof of the stereoselective seeding process for the synthesis of conglomerates was further characterized by measuring the melting curves of the resultant seeded solutions. Hence, formation of conglomerates after heterochiral seeding (T_e = 330 K, [**(S)-1$_{Seed}$**] = [**(R)-1$_M$**] = 5 × 10^{-5} M) showed a similar critical elongation temperature (T_e) with respect to only **(R)/(S)-1** homopolymer (T_e = 329 K, [**(S)-1**] = 5 × 10^{-5} M). Whereas the formed block co-polymer after homochiral seeding reveals an increased in critical elongation temperature (T_e = 342 K, [**(S)-1$_{Seed}$**] = [**(S)-1$_M$**] = 5 × 10^{-5}

M). This is due to elongation of **(S)-1$_M$** monomers on both the termini of seed (**(S)-1$_{Seed}$**) increases the effective degree of polymerization and thereby, the thermal stability.[1]

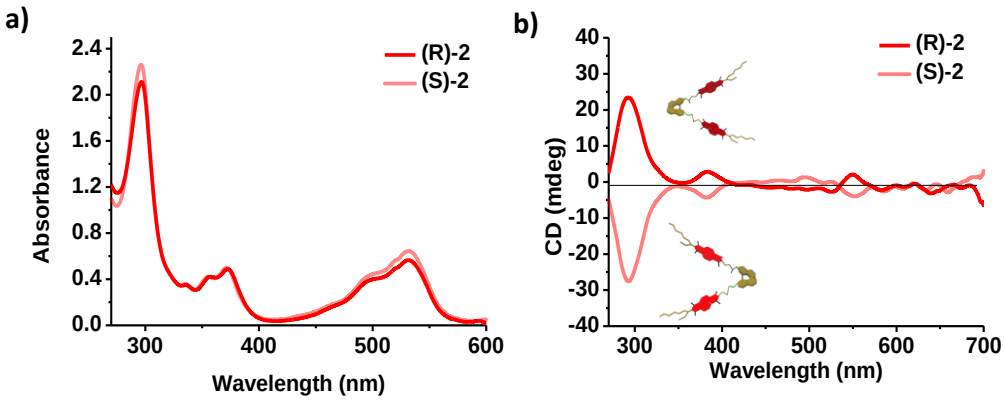

Figure S5. a) Absorption spectra and b) Mirror-image CD spectra of **(R)-2** and (**S)-2** in tetrachloroethane (TCE). ([**(R)-2**] = [**(S)-2**] = 2.5 × 10^{-5} M, l = 10 mm, 25 ºC)

Note: Both the enantiomers exhibit sharp π-π* and n-π* absorption band characteristic of cNDI chromophores in its monomeric state (**(R)/(S)-2**: $\lambda_{max\ (\pi-\pi^*)}$ = 372 nm, $\lambda_{max\ (n-\pi^*)}$ = 532 nm; (**S)-3**: $\lambda_{max\ (\pi-\pi^*)}$ = 364 nm, $\lambda_{max\ (n-\pi^*)}$ = 470 nm). Further both monomers exhibited weak exciton coupled CD signals with a zero-crossing at 535 nm and 405 nm due to the intra-chromophoric interactions characteristic of bischromophoric systems.[6-7]

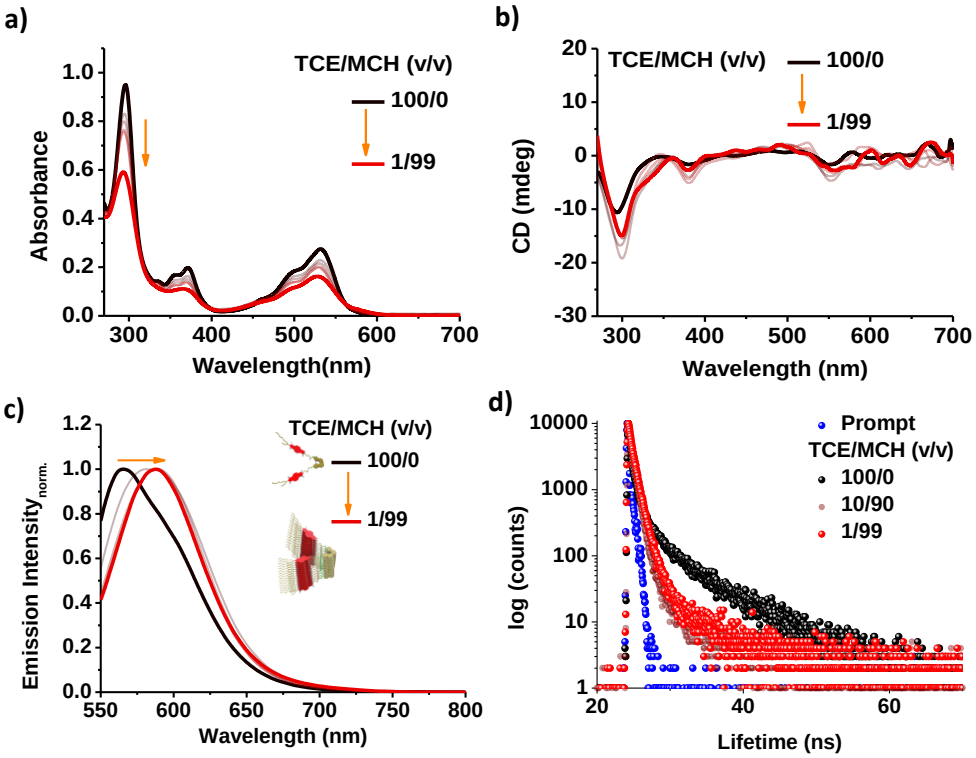

Figure S6. Solvent composition-dependent self-assembly study of (**S**)-**2**. a) Absorption, b) CD, and c) emission spectra of (**S**)-**2** by varying the % of TCE/MCH solvent composition. d) Fluorescence lifetime decay profile of (**S**)-**2** in molecularly dissolved state, TCE and self-assembled state, TCE/MCH solvent mixture (Table S2). ([(**S**)-**2**] = 2.5 × 10^{-5} M, l = 10 mm, 25 ºC, λ_{exc} = 480 nm, λ_{coll} = 650 nm)

Note: On increasing percentage of MCH in TCE/MCH solvent mixtures, the reversal of intensity of vibronic peaks at the π-π* absorption band ($A_{370\ nm}/A_{355\ nm}$ = 1.04) was observed and the corresponding CD spectra also becomes red-shifted. Supramolecular homopolymer of **(S)-2,** showed a red-shifted emission (Δλ = 23 nm) in self-assembled state (λ_{max} = 588 nm) compared to the molecularly dissolved form (λ_{max} = 565 nm) in TCE. The changes in fluorescence lifetime in monomeric and homopolymeric state suggest the emissive nature of the aggregated state. Briefly, the relative population of the shorter lifetime species increases and higher lifetime species decreases while going from molecularly dissolved state to homopolymeric state.

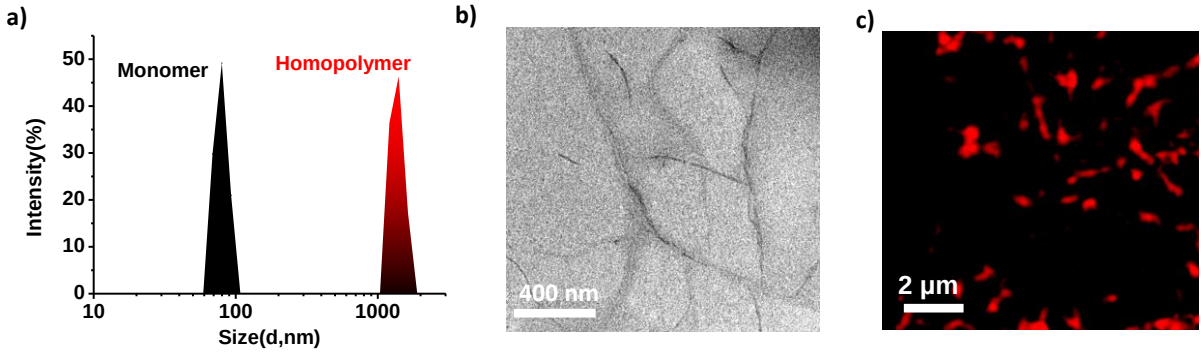

Figure S7. Morphological characterization of homopolymer, **(S)-2**. a) Intensity percentage dynamic light scattering size of (**S)-2** showing a higher hydrodynamic radius for homopolymeric state (TCE/MCH, 1/99 (v/v)) in comparison to molecularly dissolved state (TCE). Microscopic b) TEM, and c) SIM images of homopolymeric state of (**S)-2**. ([**(S)-2**] = 2.5 × 10^{-5} M, TCE/MCH, 1/99 (v/v), channel II: λ_{exc} = 561 nm, λ_{coll} = 570 nm-650 nm)

Note: From the morphological characterization, it is evident that homopolymers of **(S)-2** forms one-dimensional, red-emissive fibrous structures. Due to shorter length of the supramolecular polymer of **(S)-2**, the fluorescence SIM imaging is not well-resolved, rather in few places it shows spherical objects. It is worth mentioning that as the theory of Dynamic Light Scattering (DLS) is based on spherical particles, the obtained results in DLS can only be utilized to show the qualitative trend and not to extract any quantitative sizes.

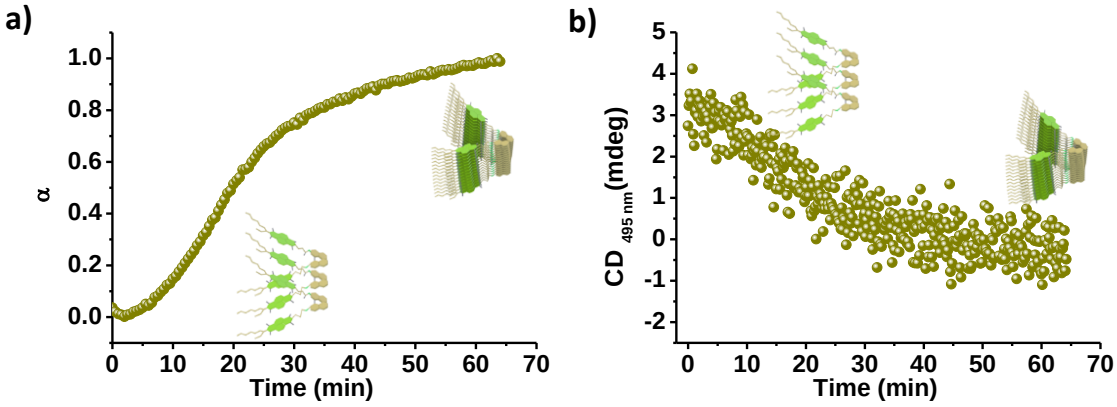

Figure S8. Kinetically controlled growth of **(S)-3** monomers obtained by monitoring the changes in a) absorbance and b) CD intensity at 495 nm. (α = degree of polymerization, [**(S)-3**] = 2.5 × 10^{-5} M, TCE/MCH, 1/99 (v/v), 25 ºC, 10 mm)

Note: On introduction of TCE stock of **(S)-3** monomers into MCH solvent a time-dependent supramolecular polymerization process was observed, rather than a spontaneous self-assembly as observed for the monomers of **2**. Therefore, spectroscopic probing of the self-assembly process, by monitoring the absorbance changes and CD changes at 495 nm, showed a non-linear growth curve

with a lag-phase, t_{lag} of 3.8 min, characteristic of a kinetically controlled cooperative supramolecular homopolymerization process.

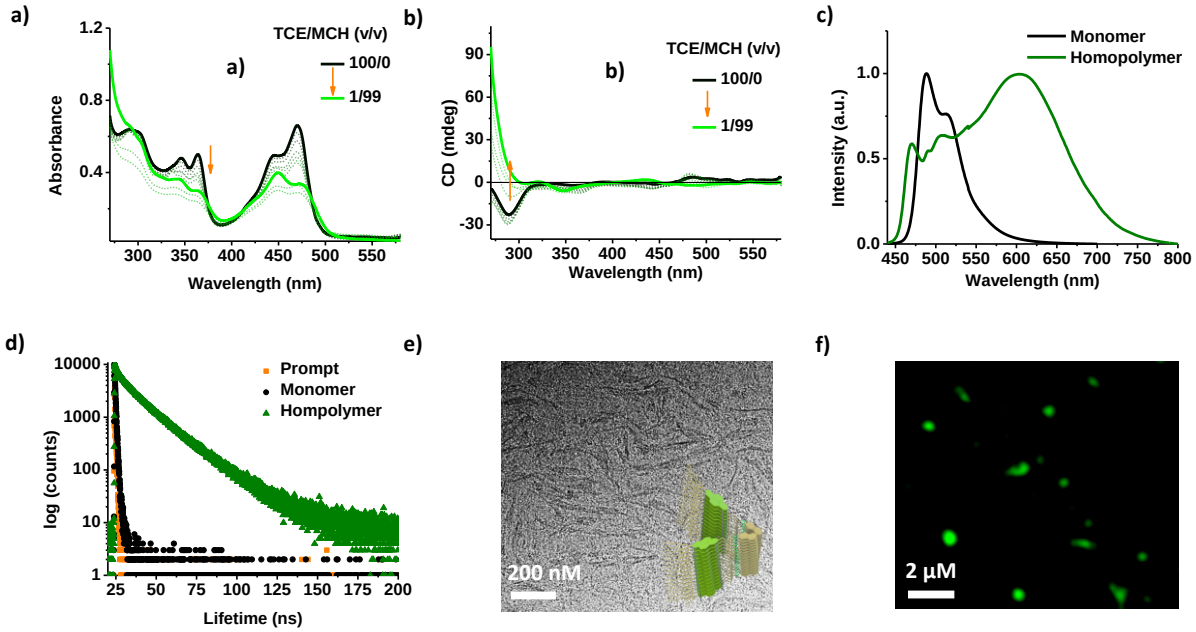

Figure S9. Solvent composition-dependent self-assembly study of (**S)-3:** a) Absorption and b) CD spectra by varying the % of TCE/MCH solvent composition. c) Emission spectra (λ_{exc} = 430 nm), d) excitation (λ_{coll} = 470 nm for monomer; λ_{coll} = 650 nm for homopolymer), and d) fluorescence lifetime decay profile (λ_{exc} = 442 nm, λ_{coll} = 570 nm for monomer; λ_{coll} = 650 nm for homopolymer) of (**S)-3** in monomeric state in TCE and self-assembled state in TCE/MCH, 1/99 (v/v) solvent mixture (table S3). e) Negatively stained TEM images, and f) SIM images of **(S)-3** homopolymer (channel I: λ_{exc} = 488 nm, λ_{coll} = 495 nm-575 nm) in TCE/MCH, 1/99 (v/v) solvent mixture. ([**(S)-3**] = 2.5 × 10^{-5} M, l = 10 mm, 25 ºC)

Note: With an incremental percentage of MCH in TCE/MCH solvent mixtures, the intensity ratio of vibronic transition of π-π* (346 nm and 364 nm) and n-π* (444 nm and 470 nm) absorbance band changes along with a clear red-shift of 5 nm in n-π* band, suggesting the aggregation of chromophores. The CD spectra shows bisignated CD signal with a zero-crossing at 402 nm and 450 nm in 1/99, TCE/MCH (v/v) solvent mixtures. The presence of CD signal even in molecularly dissolved state suggests towards the intramolecular excitonic coupled chromophores. The red-shifted, structure-less emission in the homopolymeric state suggests the formation of excimers, which could be further characterized with time-resolved fluorescence studies (lifetime, $\tau_{excimer}$ = 16 ns).

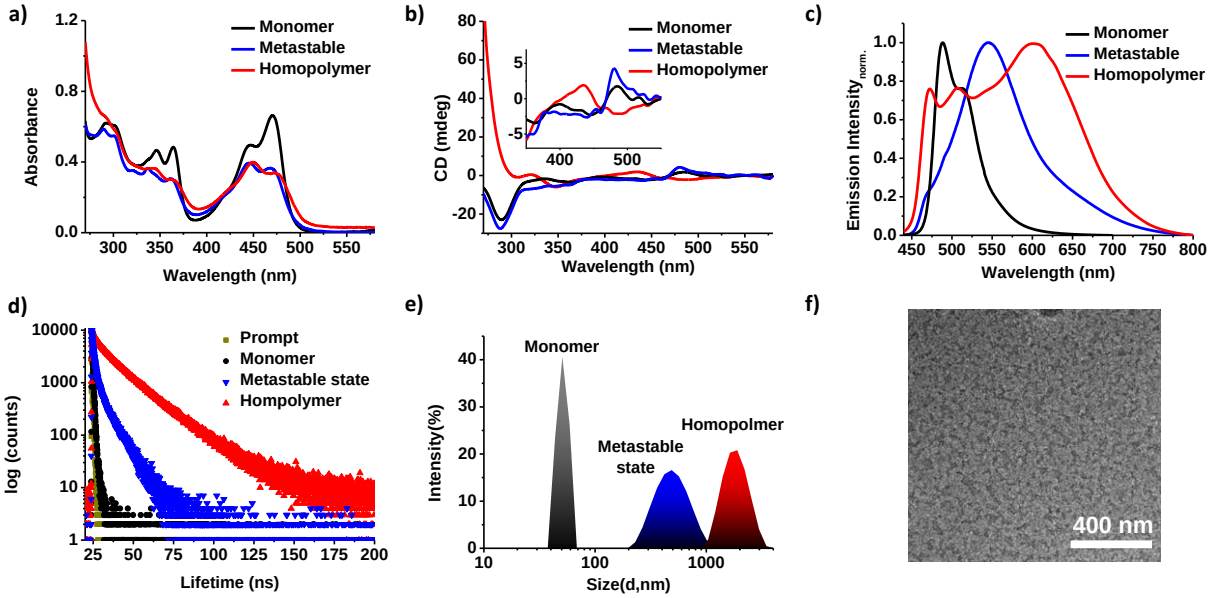

Figure S10. Pathway complexity in the self-assembly of **(S)-3**. Spectral characteristics of monomer, metastable state, and homopolymer in TCE/MCH, 1/99 (v/v) solvent mixture for (**S)-3** enantiomer**.** a) Absorption spectra, b) CD spectra (Inset: zoomed-in CD spectra between 350 nm-550 nm), c) emission profile (λ_{exc} = 430 nm), d) fluorescence lifetime decay profile (λ_{exc} = 442 nm, λ_{coll} = 470 nm for monomer; λ_{coll} = 530 nm for metastable state; λ_{coll} = 650 nm for homopolymer) (table S3), and e) Intensity percentage dynamic light scattering size of monomer in TCE, metastable and homopolymeric state in TCE/MCH, 1/99 (v/v) solvent mixture. f) Negatively stained (0.1 % uranyl acetate, (v/v)) TEM image of metastable state in TCE/MCH, 3/97 (v/v) solvent mixture showing the presence of ill-defined aggregates. ([**(S)-3**) = 2.5×10^{-5} M, l = 10 mm, 25 ºC)

Note: From the absorption spectra, it is evident that the metastable state shows a distinct absorption feature of the π-π* vibronic bands (ratio of absorbance; $A_{0\text{-}1(344\ nm)}/A_{0\text{-}2(336\ nm)}$ = 0.91) in comparison to monomer form ($A_{0\text{-}1(346\ nm)}/A_{0\text{-}2(336\ nm)}$ = 1.12), which got gradually red-shifted and broadened with time during the formation of supramolecular homopolymer ($A_{0\text{-}1(345\ nm)}/A_{0\text{-}2(336\ nm)}$ = 1.00). The CD spectrum of metastable state shows a positive cotton effect with a maximum at 480 nm compared to its homopolymer. The corresponding emission profiles (monomer, λ_{max} = 488 nm, metastable state, λ_{max} = 546 nm, and homopolymer state, λ_{max} = 602 nm), and time-resolved fluorescence studies were also markedly different for metastable state which reiterates the presence of pathway complexity during the self-assembly of (**S)-3**. Intensity percentage dynamic light scattering size and negatively stained TEM image of metastable state show a presence of ill-defined aggregated species.

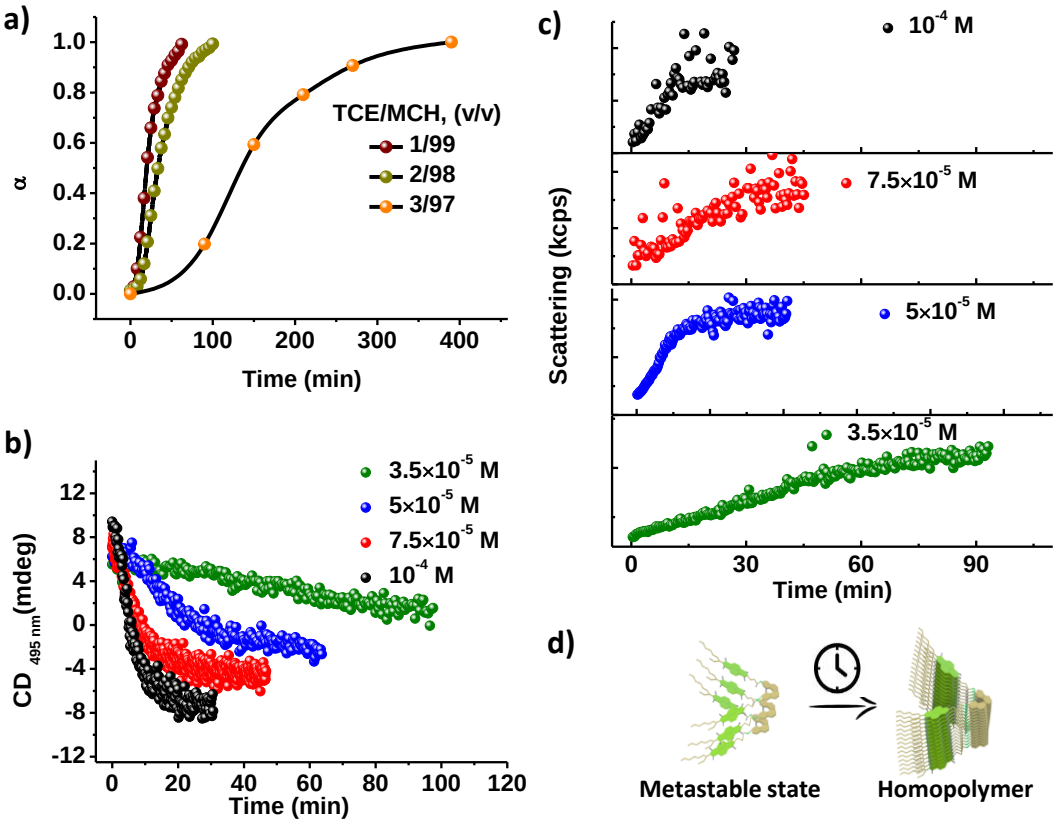

Figure S11. a) Solvent composition-dependent kinetics monitored at 495 nm absorbance band for (**S)-3** suggesting the increase in lag phase (t_{lag}) with increasing percentages of TCE (1% - 3%) in TCE/MCH solvent mixture (**[S]-2**] = 2.5 × 10^{-5} M). Concentration-dependent kinetic obtained by monitoring the b) CD band ($\lambda_{monitored}$ = 495 nm), and c) scattering which shows the conversion of metastable state to homopolymer in TCE/MCH, 3/97 (v/v) solvent mixture profiles ((**[S]-2**] = 3.5 × 10^{-5} M - 10^{-4} M). ((a) represents relative growth kinetics of **(S)-3** homopolymer assuming the extent of aggregation is zero at t = 0 min. d) Schematic representation of kinetically controlled supramolecular homopolymerization of **(S)-3**. (l = 10 mm, 25 ºC)

Note: The composition-dependent growth kinetics suggests that with increasing percentages of TCE (solvent where molecule remains as molecularly dissolved state), half-time (t_{50}) increases indicating lesser stability of intermolecularly hydrogen-bonded homopolymer (c = 2.5 × 10^{-5} M; TCE/MCH (v/v), t_{50} = 1/99, 19.8 min; 2/98, 33.9 min; 3/97, 135.2 min). Further, concentration-dependent growth kinetics for **(S)-3** monomer in TCE/MCH, 3/97 (v/v) shows a similar growth pattern as monitored by absorbance, CD, and scattering. With increasing the monomer concentration, the lag phase (t_{lag}) decreases which designate an ON-pathway (consecutive pathway) formation of metastable state *en route* to supramolecular homopolymers.

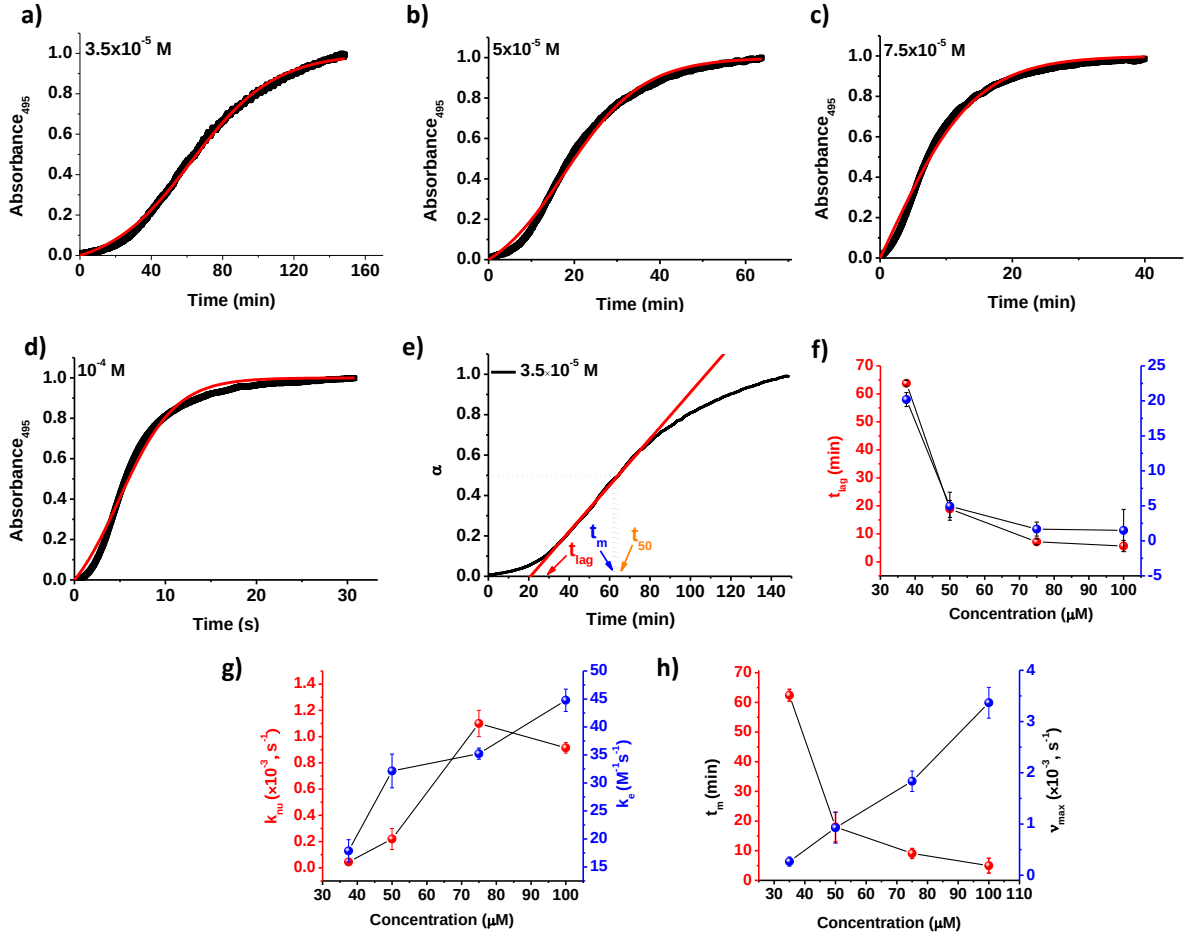

Figure S12. Fitting of time-dependent nucleation-elongation growth kinetics of **(S)-3** (kinetic data obtained from main text, figure 2f) into Watzky-Finke model[8] at various monomer concentrations: a) 3.5×10^{-5} M, b) 5×10^{-5} M, c) 7.5×10^{-5} M, and d) 10^{-4} M. e) Extraction of kinetic parameters after fitting the growth kinetics (figure S12a-d): lag time (t_{lag}), half-time (t_{50}) i.e. time required for the completion of 50% self-assembly process, t_m i.e. time at which the growth rate reaches its maximum (ν_{max}). The t_m is calculated by plotting first order derivative of the growth kinetics and then taking the maximum peak point (t_m). Plots f) t_{lag}, t_{50}, g) nucleation rate (k_{nu}), elongation rate constant (k_e), and h) t_m and ν_{max} versus (**S)-3** monomer concentration. (TCE/MCH, 3/97 (v/v), l = 10 mm)

Note: With increasing the monomer concentration, the kinetic parameters like t_{lag}, t_{50}, t_m decreases which corroborates the "ON-pathway" supramolecular polymerization process. This also indicates the increase in nucleation rate (k_{nu}), elongation rate (k_e), and growth rate (ν_{max}) with increasing monomer concentration.

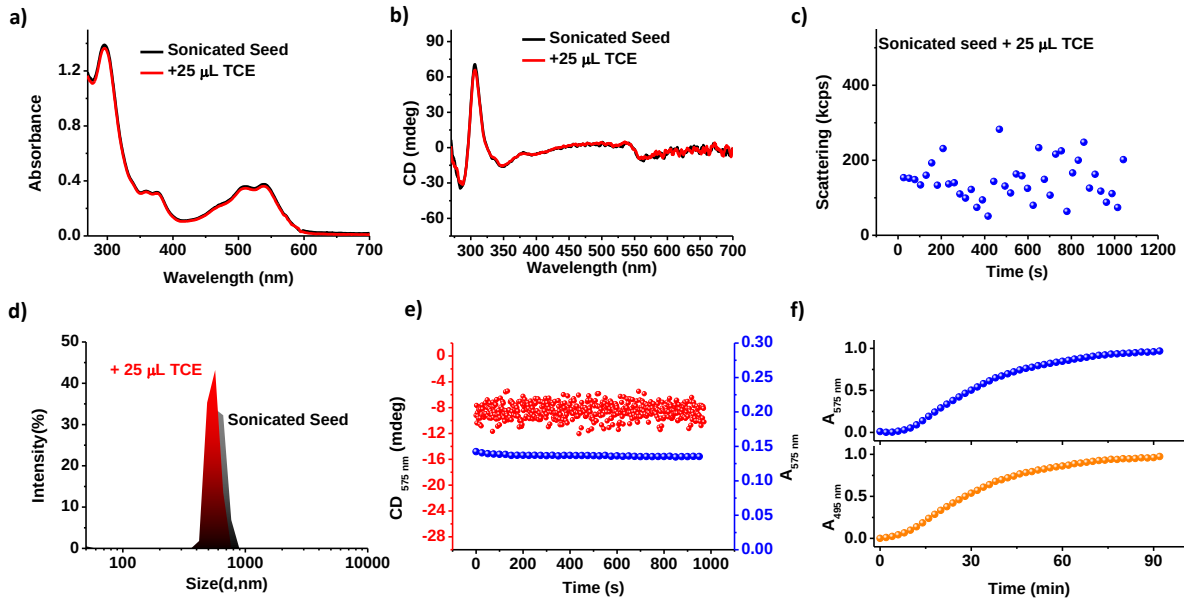

Figure S13. Control experiments to assess the kinetic stability of **(S)-2**$_{\mathbf{Seed}}$. Plot of a) absorption, b) CD spectra, c) scattering kinetics for a period of 20 minutes, and d) intensity percentage dynamic light scattering size of (**S)-2**$_{\mathbf{Seed}}$ before and after addition of TCE solvent (25 µL) in TCE/MCH, 3/97 (v/v) solvent mixture. e) Time-dependent absorbance and CD kinetics of (**S)-2**$_{\mathbf{Seed}}$ in TCE/MCH, 3/97 (v/v) solvent mixture monitored at 575 nm indicating no changes in absorbance and CD signal for a period of 20 minutes. f) Kinetically controlled growth of **(S)-3** monomers by monitoring the absorbance band at 495 nm and 575 nm. (([**(S)-2**$_{\mathbf{Seed}}$] = 3.5 × 10^{-5} M, [**(S)-3**] = 3.5 × 10^{-5} M, TCE/MCH, 3/97 (v/v), 25 ^{o}C, 10 mm)

Note: This suggests the kinetic stability of sonicated seed of **(S)**-2$_{\mathbf{Seed}}$ even after addition of 25 µL of TCE (solvent where the molecule remains as a molecularly dissolved state). Therefore, on injecting the TCE stock of feed monomer (**(S)-3**$_{\mathbf{M}}$) will not affect the homochiral or heterochiral seeding kinetics. Moreover, no change in absorbance/CD signal at 575 nm reiterates high kinetic stability of **(S)**-2$_{\mathbf{Seed}}$ over a period of 20 minutes. Similar growth kinetics profiles with identical lag phase were observed for **(S)-3**$_{\mathbf{M}}$ feed monomer at 495 nm and 575 nm absorbance band. Since there is no change of **(S)**-2$_{\mathbf{Seed}}$ kinetics at 575 nm band with time, the homochiral and heterochiral seeding study during the multicomponent supramolecular copolymerization was monitored at 575 absorbance band to get a proper seeded growth kinetics.

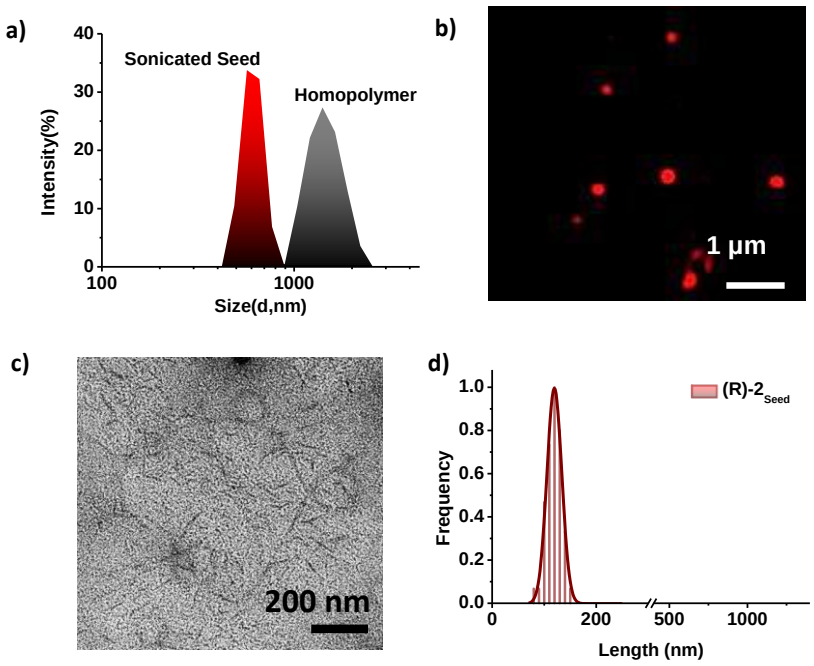

Figure S14. a) Intensity percentage dynamic light scattering size of (**S**)-**2** homopolymer and seed solution ((**S**)-$\mathbf{2_{Seed}}$) after sonication for 5 minutes in TCE/MCH, 3/97 (v/v) solvent mixture. b) SIM images of (**S**)-$\mathbf{2_{Seed}}$ seed solution after sonication for 5 minutes. c) Negatively stained TEM image, and its d) length distribution analysis of seed solution ((**R**)-$\mathbf{2_{Seed}}$) (no. of fibers counted for analysis = 70, L_n = 118 nm, L_w = 120 nm, PDI = 1.01) after sonication for 5 minutes in TCE/MCH, 3/97 (v/v) solvent mixture ([(**S**)-$\mathbf{2_{Seed}}$] = ([(**R**)-$\mathbf{2_{Seed}}$] = 3.5×10^{-5} M, TCE/MCH, 3/97 (v/v), l = 10 mm).

Note: Due to shorter sonicated seed (**S**)-$\mathbf{2_{Seed}}$, the SIM image is not well-resolved, rather shows a spherical type objects. On the other hand, TEM image indeed showed the one-dimensional nature of the seeds (Main text, figure 2h).

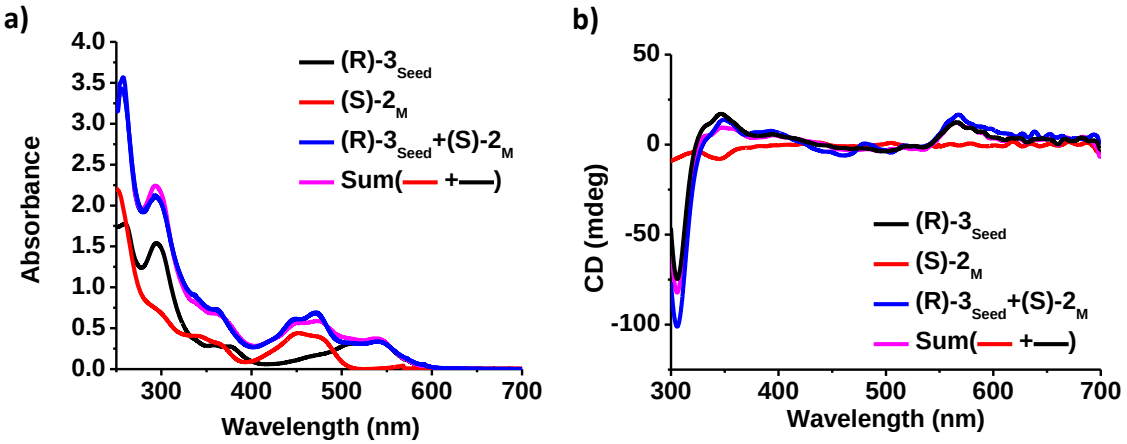

Figure S15. Spectra analysis after heterochiral-seeding experiment (Main text, figure 3c). Plots of a) absorption, and b) CD spectra of heterochiral seeded (**R**)-$\mathbf{2_{Seed}}$+(**S**)-$\mathbf{3_M}$) solutions by using (**R**)-$\mathbf{2_{Seed}}$ as

a seed solution and (**(S)-3$_M$** as a feed monomer ([**(R)-2$_{Seed}$** = [**(S)-3$_M$**] = 3.5 × 10^{-5} M, TCE/MCH, 3/97 (v/v), l = 10 mm, 25 ºC).

Note: The absorption and CD spectra for heterochiral seeding experiments signify that the resultant seeded solution **((R)-2$_{Seed}$+(S)-3$_M$))** holds overall spectral characteristics of seed, **(R)-2$_{Seed}$** and homopolymer, **(S)-2$_M$**. Additionally, summation of the absorption and CD spectrum of the individual homochiral polymers of **(R)-2**, and **(S)-3** indeed match with the heterochiral seeded self-sorted polymers **((R)-2$_{Seed}$+(S)-3$_M$))**.

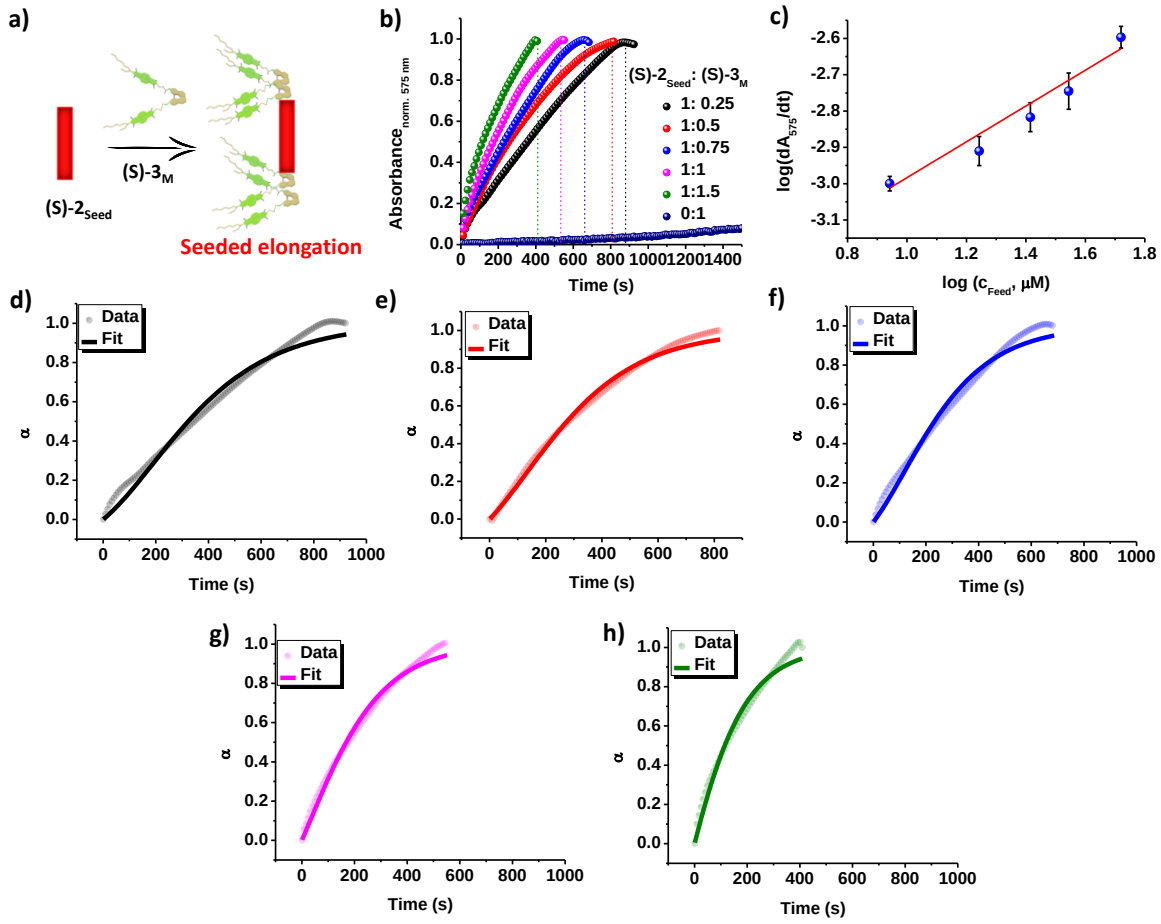

Figure S16. a) Schematic representation of homochiral seed-induced primary nucleation-elongation events using **(S)-2$_{Seed}$** as a seed solution and **(S)-3$_M$** as a feed monomer. b) Time-dependent absorbance changes monitored at 575 nm for homochiral seeded supramolecular polymerization (**(S)-2$_{Seed}$+(S)-3$_M$**) by using constant **(S)-2$_{Seed}$** concentration (3.5 × 10^{-5} M) and varying concentrations of corresponding monomer (0.8 × 10^{-6} M to 5.2 × 10^{-5} M). c) log-log plot of rate of seeded supramolecular polymerization (calculated from figure S16b) with the monomer concentration shows a linear trend with a slope of 1.02 which suggests a seeded chain-growth supramolecular polymerization process. Fitting of homochiral seeded kinetics (**(S)-2$_{Seed}$+(S)-3$_M$**) (extracted from figure 16b) into seed-induced nucleation-elongation model by using online software

http://www.amylofit.ch.cam.ac.uk at constant seed concentration ([**(S)-2**$_{\mathbf{Seed}}$] = 3.5 × 10^{-5} M) and variable feed monomer ([**(S)-3**$_{\mathbf{M}}$] concentration: d) 0.8 × 10^{-5} M, e) 1.7 × 10^{-5} M, f) 2.6 × 10^{-5} M, g) 3.5 × 10^{-5} M, and h) 5.2 × 10^{-5} M. (TCE/MCH, 3/97 (v/v), l = 10 mm, 25 ºC)

Note: The homochiral seeded solutions for variable monomer concentration showed a good-fit into seed-induced nucleation elongation model with a MSE less than 0.0018 (table S4).[5]

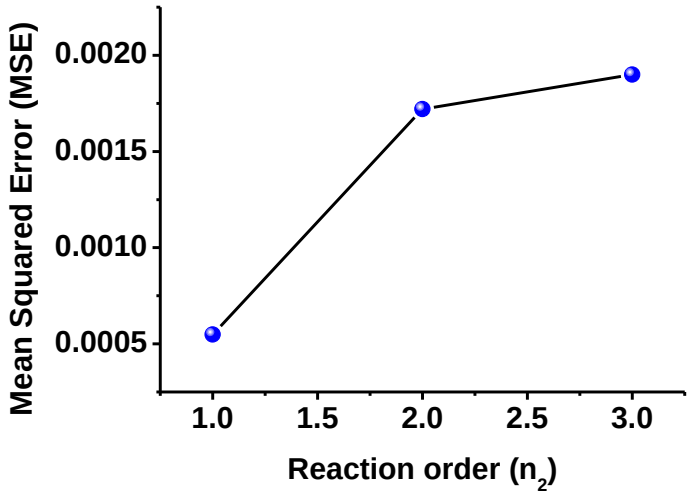

Figure S17. Effect of reaction order (n_2) on the error of fitting with secondary nucleation model. This indicates with increasing reaction order, the mean squared error (MSE) increases hinting towards poor fitting of the heterochiral seeded kinetics (Main text, figure 3f). (3/97, TCE/MCH (v/v), 25 ºC, 10 mm)

Note: The reaction order (n_2) 1 with lowest MSE matches well with experimentally evaluated reaction order from the scaling exponent.

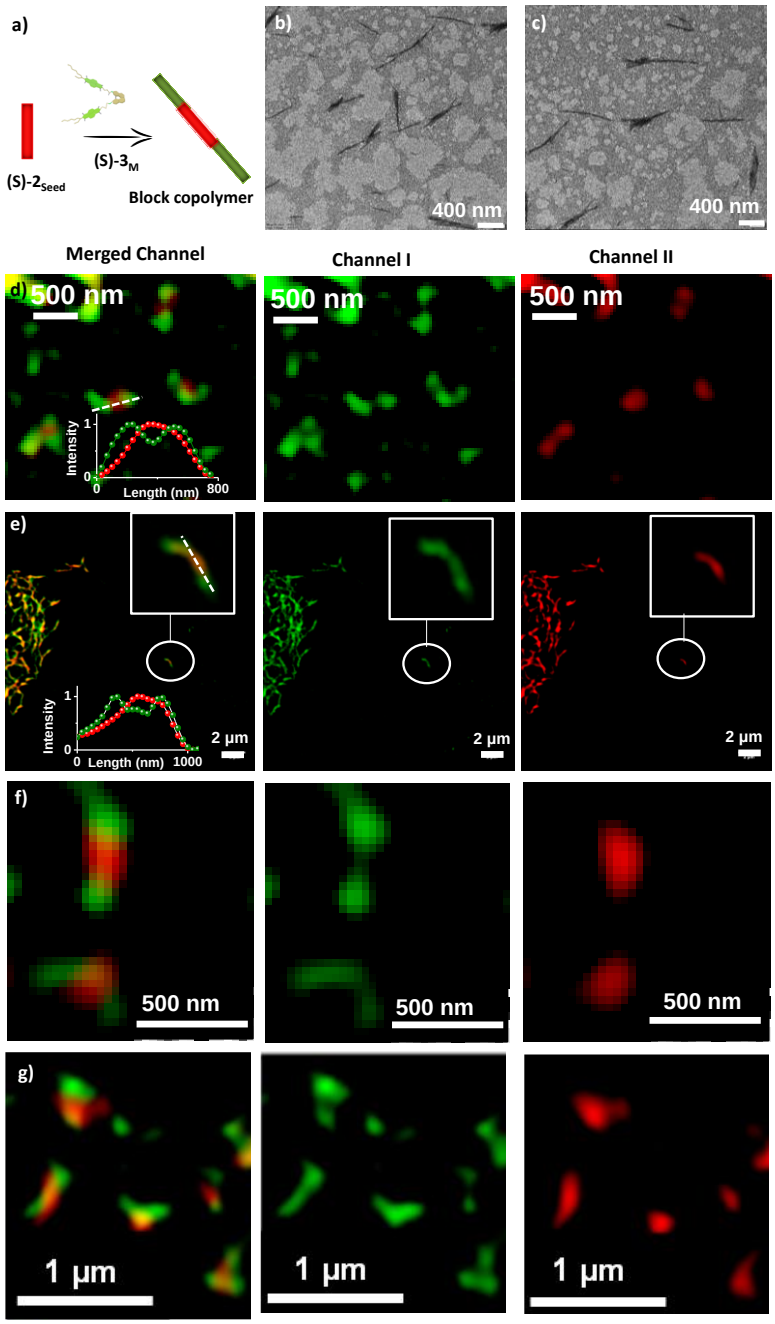

Figure S18. a) Schematic representation of primary nucleation-elongation events during the homochiral seeded supramolecular co-polymerization, using **(S)-2$_{Seed}$** as a seed and **(S)-3$_M$** as a feed monomer. b,c) TEM, and d-g) SIM images of homochiral seeded (**(S)-2$_{Seed}$+(S)-3$_M$**) solutions suggests the formation of supramolecular block co-polymers. Inset plots in figure (d) and (e) show the intensity profile of block co-polymer where the seed (**(S)-2$_{Seed}$**) locates in the middle portion and monomer (**(S)-3$_M$**) elongates from both end of the seed. ([**(S)-2$_{Seed}$**] = [**(S)-3$_M$**] = 3.5×10^{-5} M, TCE/MCH, 3/97 (v/v), l = 10 mm, channel I: λ_{exc} = 488 nm, λ_{coll} = 495 nm-575 nm, channel II: λ_{exc} = 561 nm, λ_{coll} = 570 nm-650 nm)

Note: TEM images of the supramolecular co-polymers obtained after the homochiral seeding (**(S)-2$_{Seed}$+(S)-2$_M$**) shows an increase in average length compared to that of the nascent seeds of **(S)-2$_{Seed}$**

(Main text, figure 4b,c). This is in agreement with a primary nucleation-elongation driven seeded supramolecular polymerization process. The corresponding SIM images seeded supramolecular copolymers obtained by the homochiral seeding showed the alternate segmented organization of green (**(S)-3**) and red (**(S)-2**) blocks, suggesting the formation of a two-component supramolecular block co-polymer.

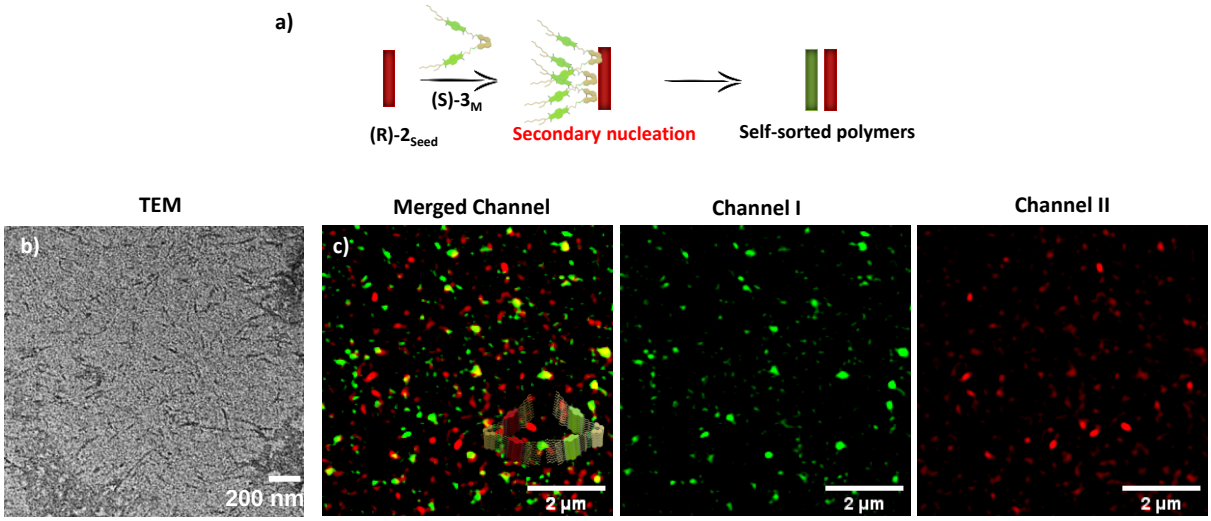

Figure S19. a) Schematic representation of secondary nucleation-elongation events during the heterochiral seeded supramolecular co-polymerization, using and **(R)-2$_{Seed}$** as a seed and **(S)-3$_M$** as a feed monomer. b) TEM, and c) SIM images of heterochiral seeded (**(R)-2$_{Seed}$+(S)-3$_M$**)) solutions suggests the formation of supramolecular self-sorted polymer. ([**(R)-2$_{Seed}$**] = [**(S)-3$_M$**] = 3.5×10^{-5} M, TCE/MCH, 3/97 (v/v), channel I: λ_{exc} = 488 nm, λ_{coll} = 495 nm-575 nm; channel II: λ_{exc} = 561 nm, λ_{coll} = 570 nm-650 nm)

Note. TEM image of the supramolecular polymers obtained after heterochiral seeding (**(R)-2$_{Seed}$+S-3$_M$**) indicates that the average length of the supramolecular polymers is similar to that of the nascent seed (**(R)-2$_{Seed}$**) hinting the absence of any seed-induced elongation process. However, the polymer length of both the **(R)-2$_{Seed}$** and **(S)-3$_M$** are quite similar, so we couldn't observe any bimodal distribution in length for heterochiral seeding experiments (Main text, figure 4b,c). The corresponding SIM image shows the secondary nucleation triggered, attachment of green fibers of **(S)-3$_M$** on the existing red-emissive fibers of **(R)-2$_{Seed}$** seed which appears as an attached green (**(S)-3$_M$**) and red fibers (**(R)-2$_{Seed}$**) with yellow interface (green+ red).

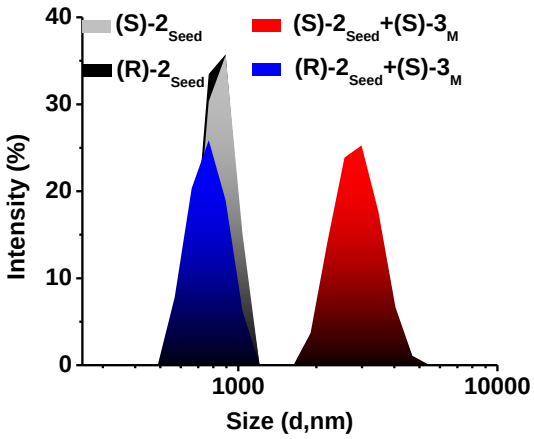

Figure S20. a) Light scattering intensity percentage dynamic light scattering size of homochiral seeded ((**S**)-**2**$_{\mathbf{Seed}}$+(**S**)-**3**$_{\mathbf{M}}$), and heterochiral seeded solutions ((**R**)-**2**$_{\mathbf{Seed}}$+(**S**)-**3**$_{\mathbf{M}}$). ([(**S**)-**2**$_{\mathbf{Seed}}$] = [(**R**)-**2**$_{\mathbf{Seed}}$] = [(**S**)-**3**$_{\mathbf{M}}$] = 3.5×10^{-5} M, TCE/MCH, 3/97 (v/v), 10 mm)

Note: From dynamic light scattering (DLS) studies, a similar hydrodynamic size for heterochiral seeded solution (d_H = 760 nm for self-sorted polymer) and increased size for homochiral seeded solution (d_H = 2800 nm for block co-polymer polymer) were observed with respect to its corresponding seed solution (d_H = 850 nm for seed) It is worth-mentioning that as DLS considers supramolecular polymers as spherical objects, so the obtained results after seeding could only be utilized as to show a trend.

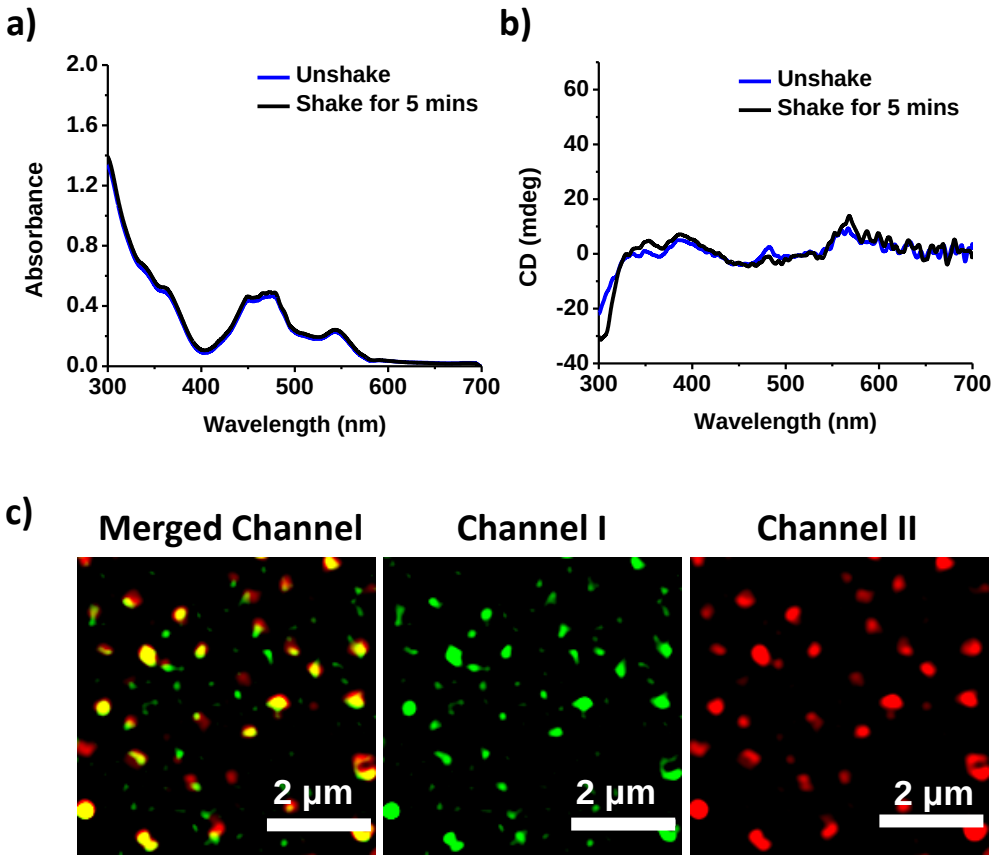

Figure S21. Spectra and microscopic analysis of heterochiral-seeding experiment. Plots of a) absorption, and b) CD spectra of heterochiral seeded **(R)-2$_{Seed}$+(S)-3$_{M}$)** solutions before and after vigorous shake (for 5 minutes) of the solutions. c) The corresponding SIM image of heterochiral seeded ((**R)-2$_{Seed}$+(S)-3$_{M}$**)) solutions without spin-coating the imaging specimen suggests the secondary nucleation triggered, more attachment of green fibers of **(S)-3$_{M}$** on the existing red-emissive fibers of **(R)-2$_{Seed}$** seed which appears as an attached green (**(S)-3$_{M}$**) and red fibers (**(R)-2$_{Seed}$**) with yellow interface (green+ red). **[(R)-2$_{Seed}$** = **(S)-3$_{M}$]** = 3.5 × 10^{-5} M, TCE/MCH, 3/97 (v/v), l = 10 mm, 25 ºC, channel I: λ_{exc} = 488 nm, λ_{coll} = 495 nm-575 nm; channel II: λ_{exc} = 561 nm, λ_{coll} = 570 nm-650 nm)

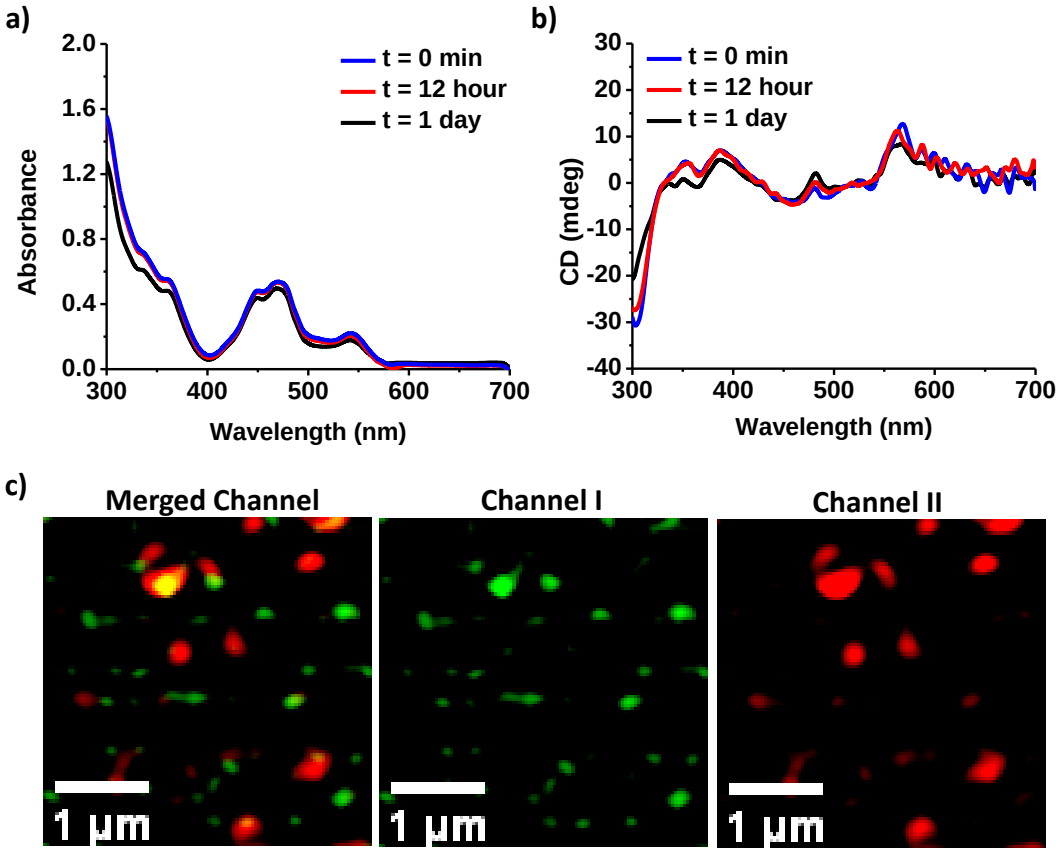

Figure S22. Kinetic stability of heterochiral-seeded self-sorted supramolecular polymers. Plots of a) absorption, and b) CD spectra of heterochiral seeded **(R)-2$_{Seed}$+(S)-3$_{M}$)** solutions over a period of 1 day suggesting similar spectral features compared to the spectral features at t = 0 minutes. c) The corresponding SIM image of heterochiral seeded ((**R)-2$_{Seed}$+(S)-3$_{M}$**)) solutions after 1 day suggests the secondary nucleation triggered, attachment of green fibers of **(S)-3$_{M}$** on the existing red-emissive fibers of **(R)-2$_{Seed}$** seed which appears as an attached green (**(S)-3$_{M}$**) and red fibers (**(R)-2$_{Seed}$**) with yellow interface (green+ red). **([(R)-2$_{Seed}$ = [(S)-3$_{M}$]** = 3.5 × 10^{-5} M, TCE/MCH, 3/97 (v/v), l = 10 mm, 25 ºC, channel I: λ_{exc} = 488 nm, λ_{coll} = 495 nm-575 nm; channel II: λ_{exc} = 561 nm, λ_{coll} = 570 nm-650 nm)

1.5 Supporting Tables

Feed monomer concentration (**(S)-1$_M$**)	Mean Squared Error (MSE)
6×10^{-6} M	0.0003
1.25×10^{-5} M	0.0007
2.5×10^{-5} M	0.0006
5×10^{-5} M	0.0005

Table S1. Tabular format of MSE of **(S)-1** homochiral seeding with varying monomer concentration obtained after fitted the seeded kinetics with seed-induced nucleation-elongation model (figure S2).

State	$\lambda_{exc.}$ (nm)	λ_{coll} (nm).	τ_1 (ns)	τ_2 (ns)	τ_3 (ns)
Monomer (TCE)	480	650	0.2 (93%)	2.2 (7%)	-
Homopolymer (1/99, TCE/MCH (v/v))	480	650	7.0 (23%)	18.2 (73%)	0.5 (4%)

Table S2. Comparison of the lifetime data in tabulated format for (**S)-2** monomer and its homopolymer (figure S6).

State	$\lambda_{exc.}$ (nm)	λ_{coll} (nm).	τ_1 (ns)	τ_2 (ns)	τ_3 (ns)
Monomer (TCE)	442	470	0.2 (93%)	2.2 (7%)	-
Metastable (1/99, TCE/MCH (v/v))	442	530	1.5 (40%)	7.9 (40%)	0.2 (20%)
Homopolymer (1/99, TCE/MCH (v/v))	442	650	7.0 (23%)	18.2 (73%)	0.5 (4%)

Table S3. Comparison of the lifetime data in tabulated format for (**S)-3** monomer, metastable state and its homopolymer (figure S10).

Feed monomer concentration (**(S)-3$_M$**)	Mean Squared Error (MSE)
0.8×10^{-5} M	0.0017
1.7×10^{-5} M	0.0006
2.6×10^{-5} M	0.0016
3.5×10^{-5} M	0.0008
5.2×10^{-5} M	0.0017

Table S4. Tabular format of MSE **(S)-2/(S)-3** homochiral cross-seeding with varying monomer concentration obtained after fitting the seeded kinetics with seed-induced nucleation-elongation model (figure S16).

1.6 Supporting Spectra

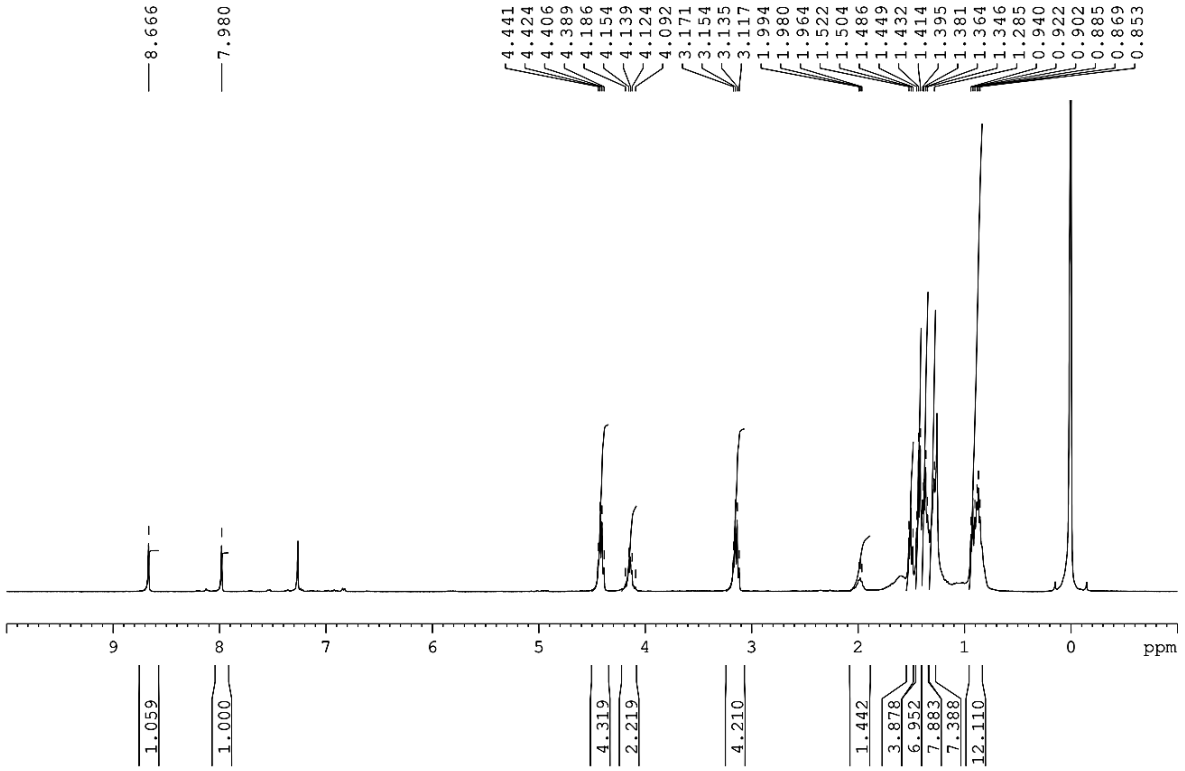

Figure S23. ^{1}H-spectrum of **6** at 25 ºC in $CDCl_3$. (BRUKER AVANCE-400 with 400 MHz)

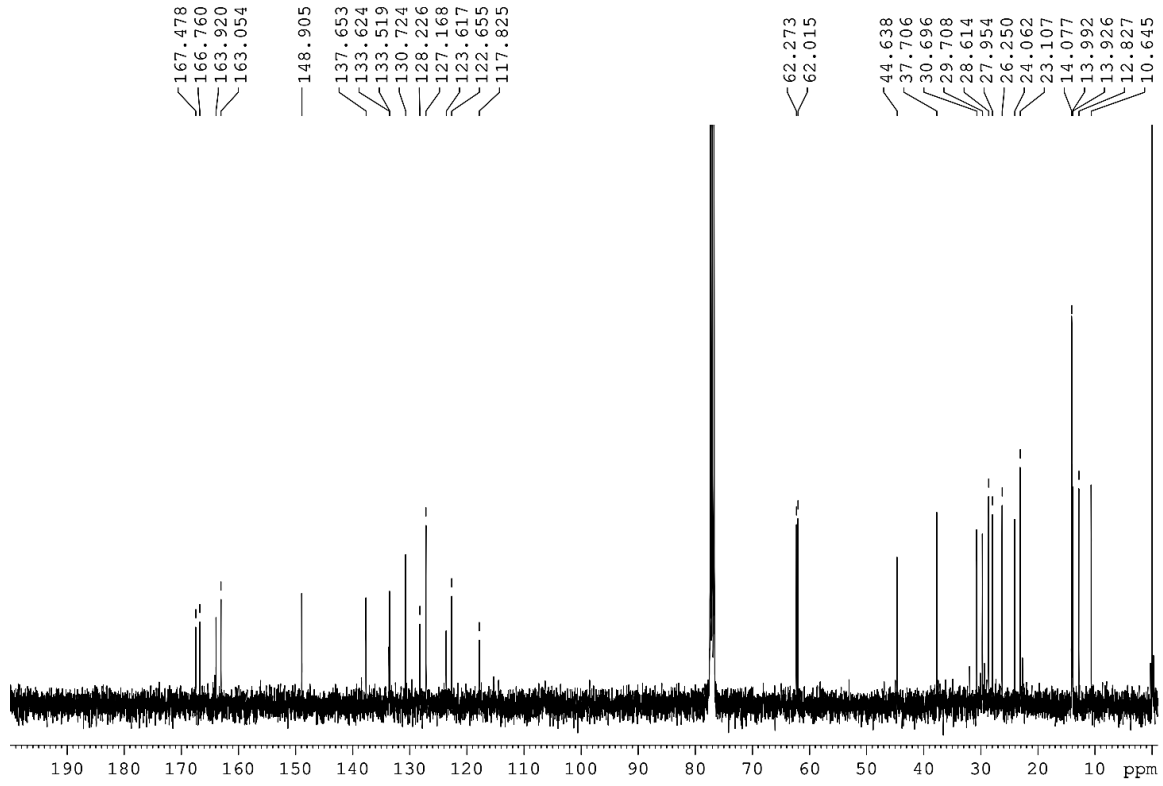

Figure S24. ^{13}C-spectrum of **6** at 25 ºC in $CDCl_3$. (BRUKER AVANCE-400 with 100 MHz)

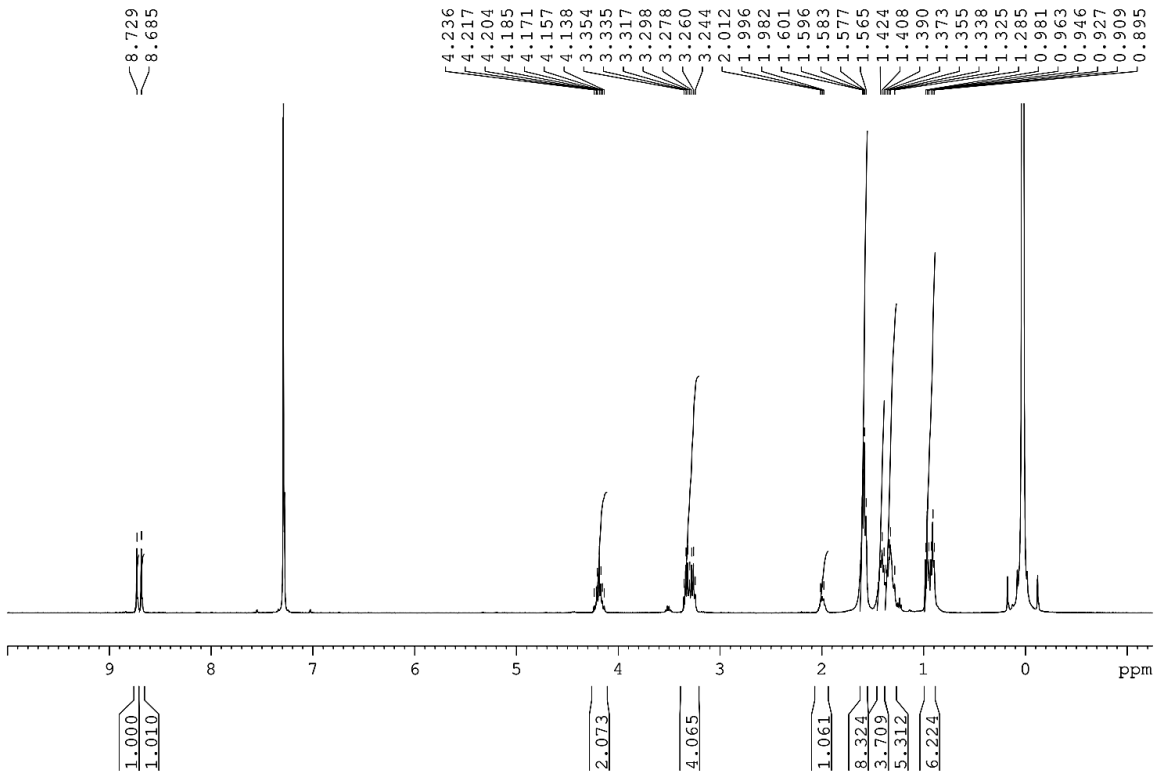

Figure S25. ^{1}H-spectrum of **7** at 25 ºC in $CDCl_3$. (BRUKER AVANCE-400 with 400 MHz)

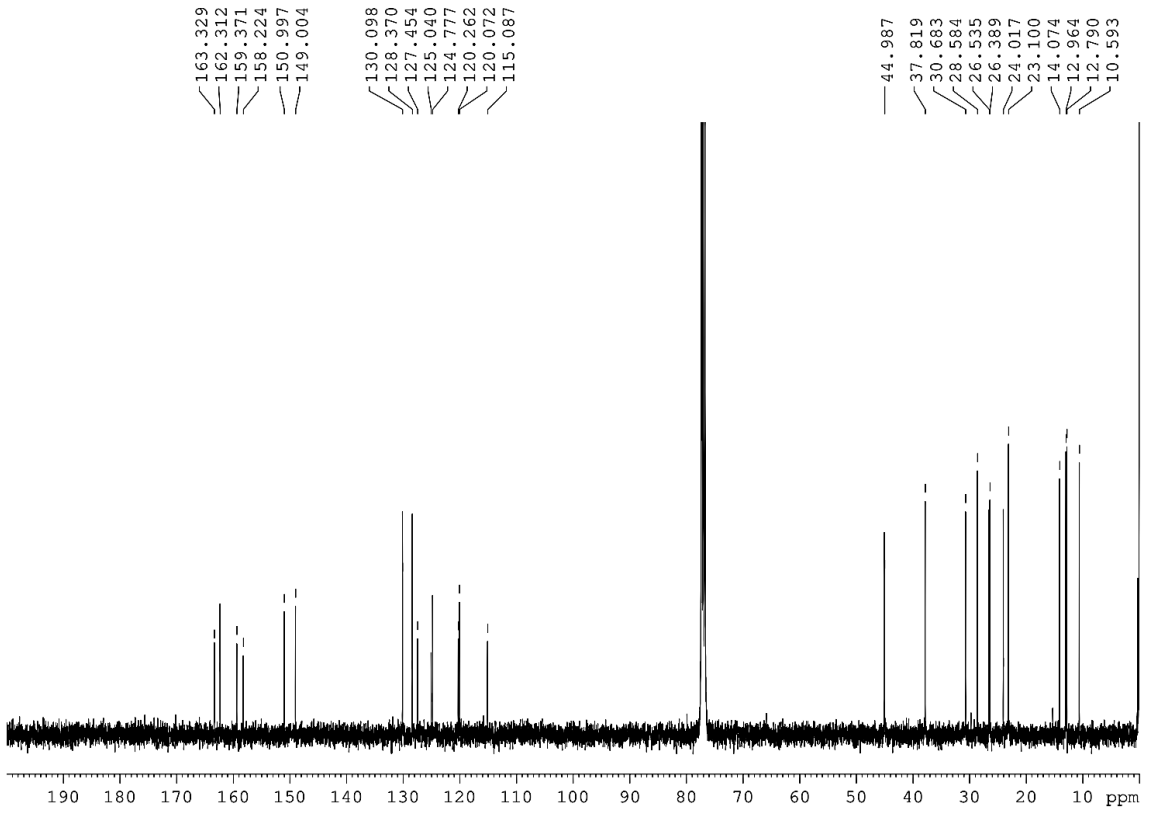

Figure S26. ^{13}C-spectrum of **7** at 25 ºC in $CDCl_3$. (BRUKER AVANCE-400 with 100 MHz)

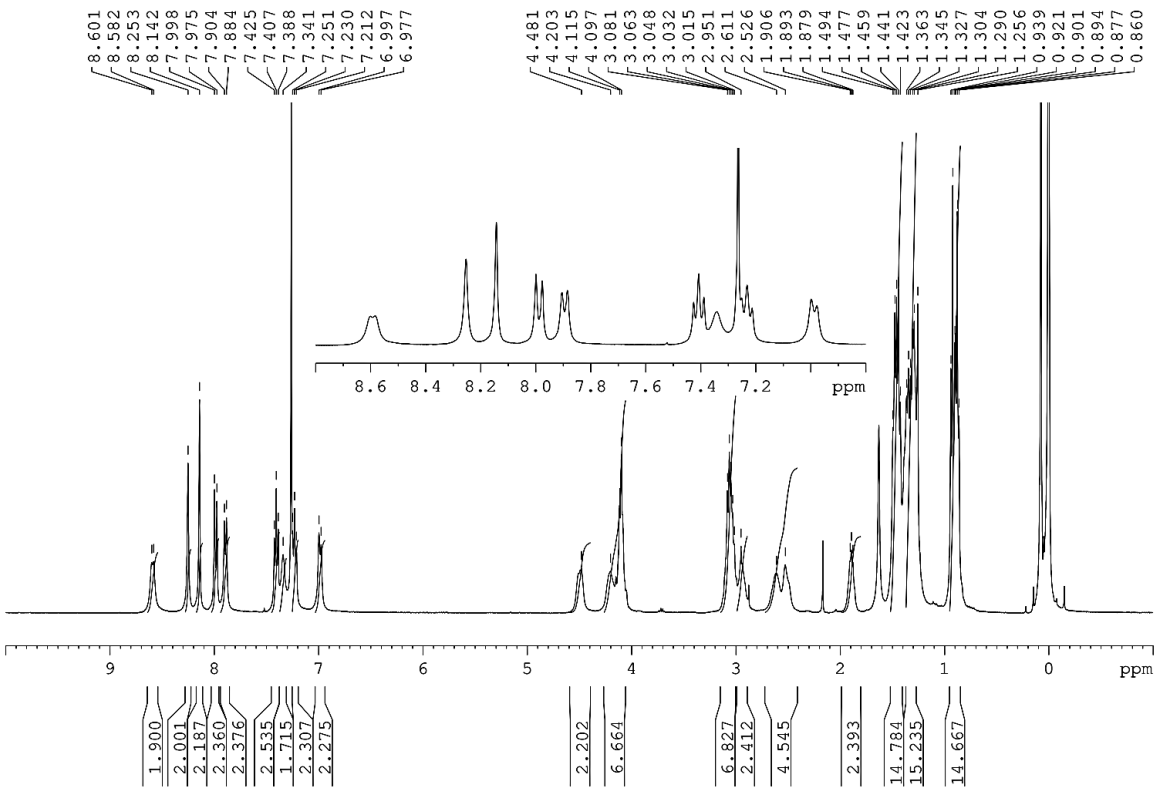

Figure S27. ^{1}H-spectrum of (**S)-2** at 25 ºC in $CDCl_3$. (BRUKER AVANCE-400 with 400 MHz)

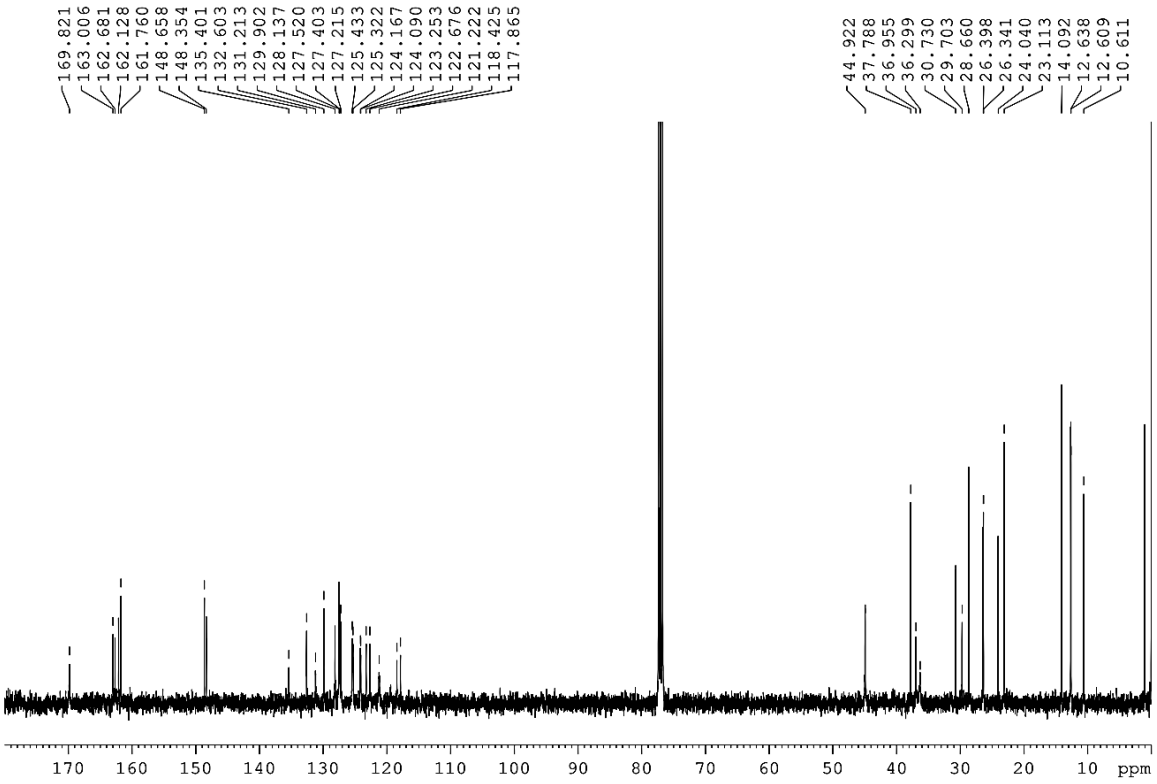

Figure 28. ^{13}C-spectrum of (**S)-2** at 25 ºC in $CDCl_3$. (BRUKER AVANCE-400 with 100 MHz)

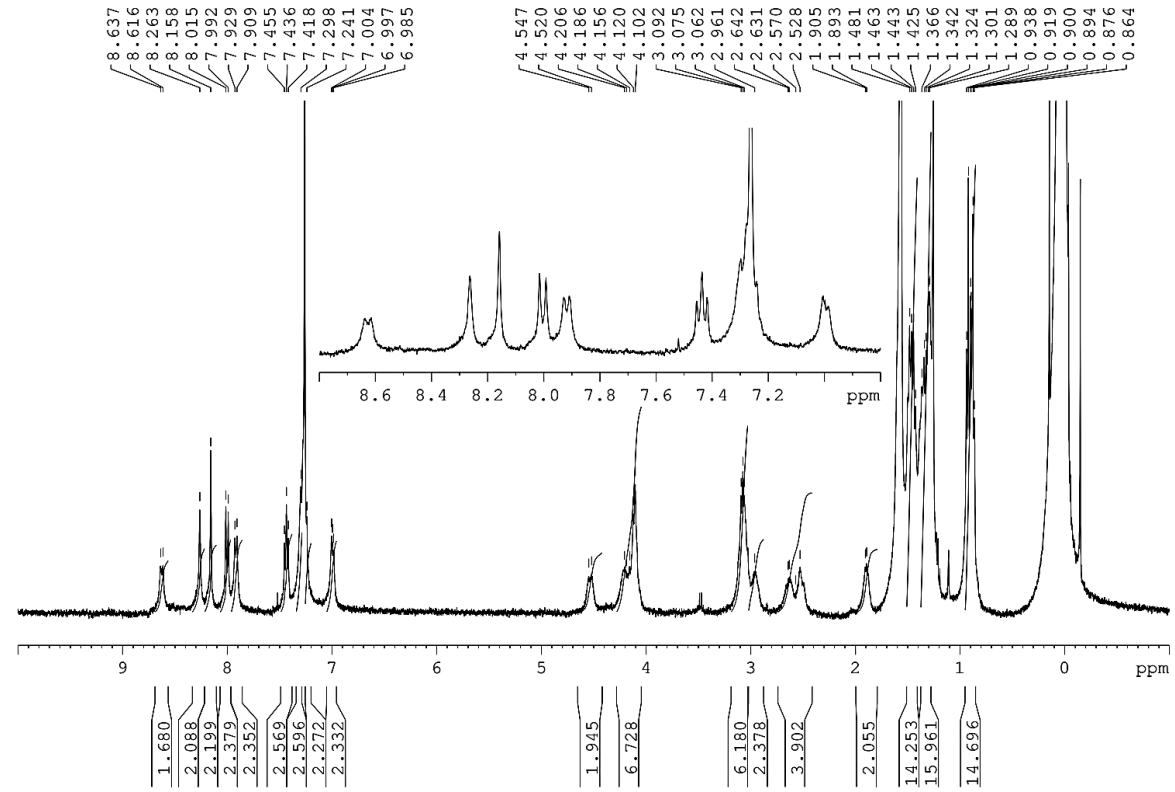

Figure S29. ^{1}H-spectrum of (**R)-2** at 25 ºC in $CDCl_3$. (BRUKER AVANCE-400 with 400 MHz)

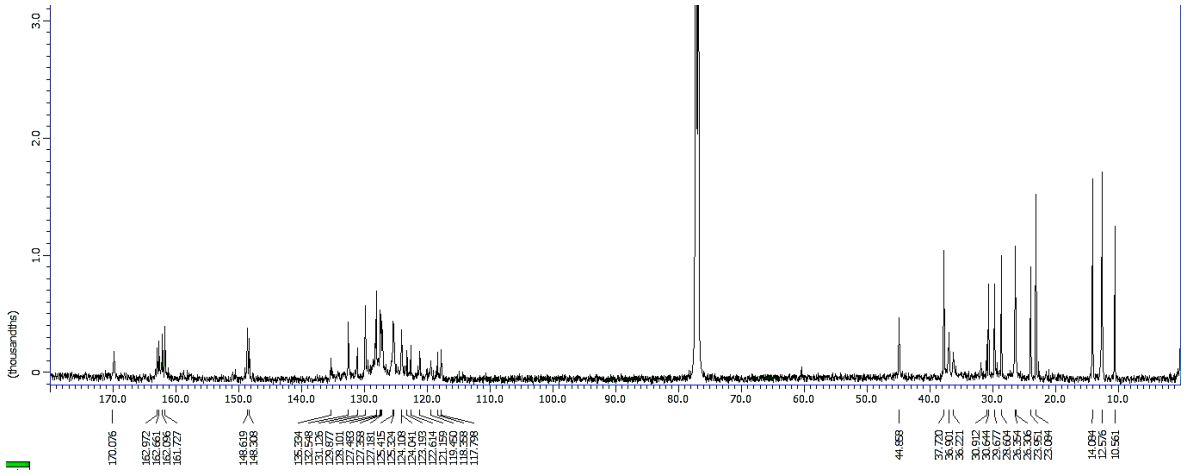

Figure S30. ^{13}C-spectrum of (**R)-2** at 25 ºC in $CDCl_3$. (JEOL-600 with 125 MHz)

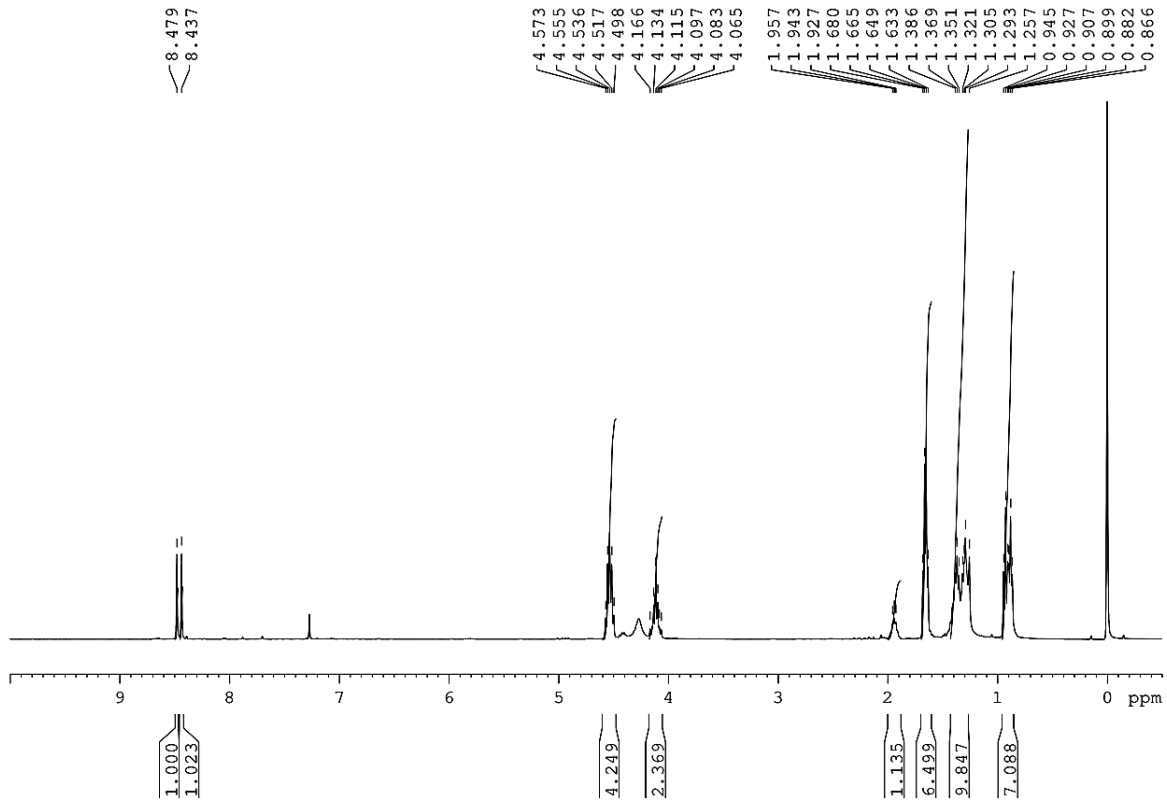

Figure S31. ^{1}H-spectrum of **12** at 25 ºC in $CDCl_3$. (BRUKER AVANCE-400 with 400 MHz)

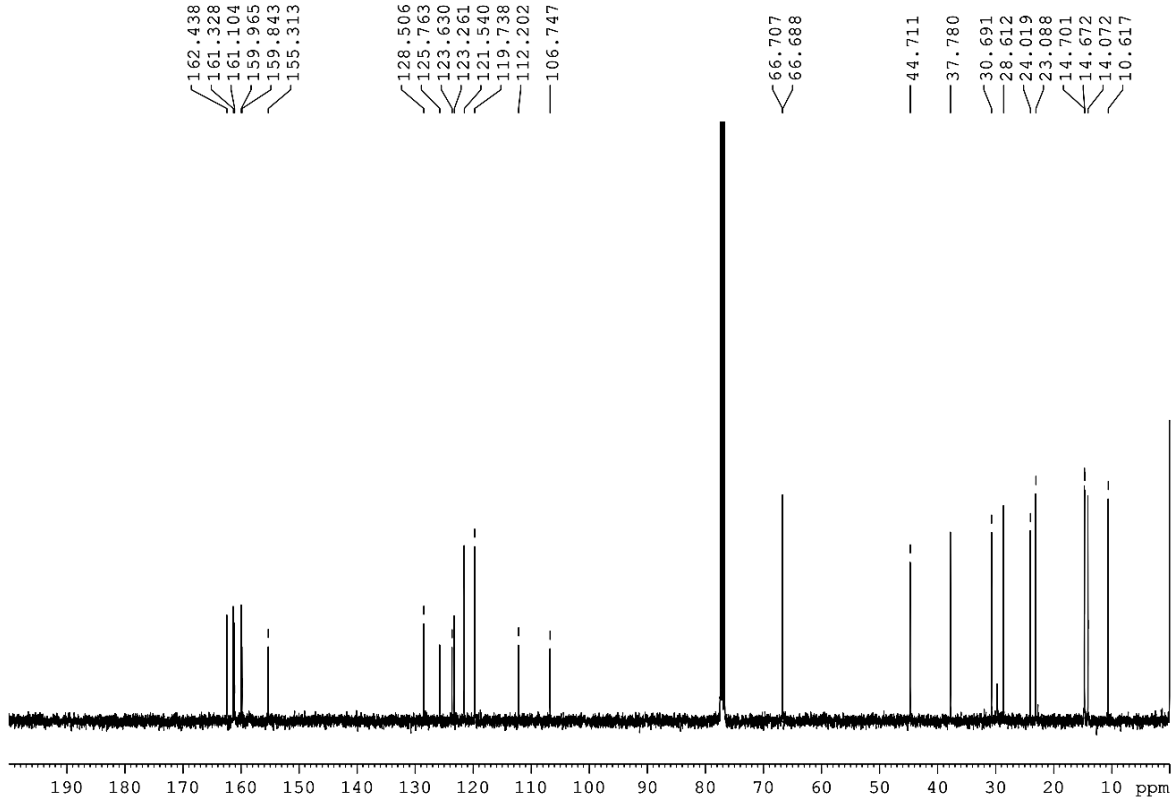

Figure S32. ^{13}C-spectrum of **12** at 25 ºC in $CDCl_3$. (BRUKER AVANCE-400 with 100 MHz)

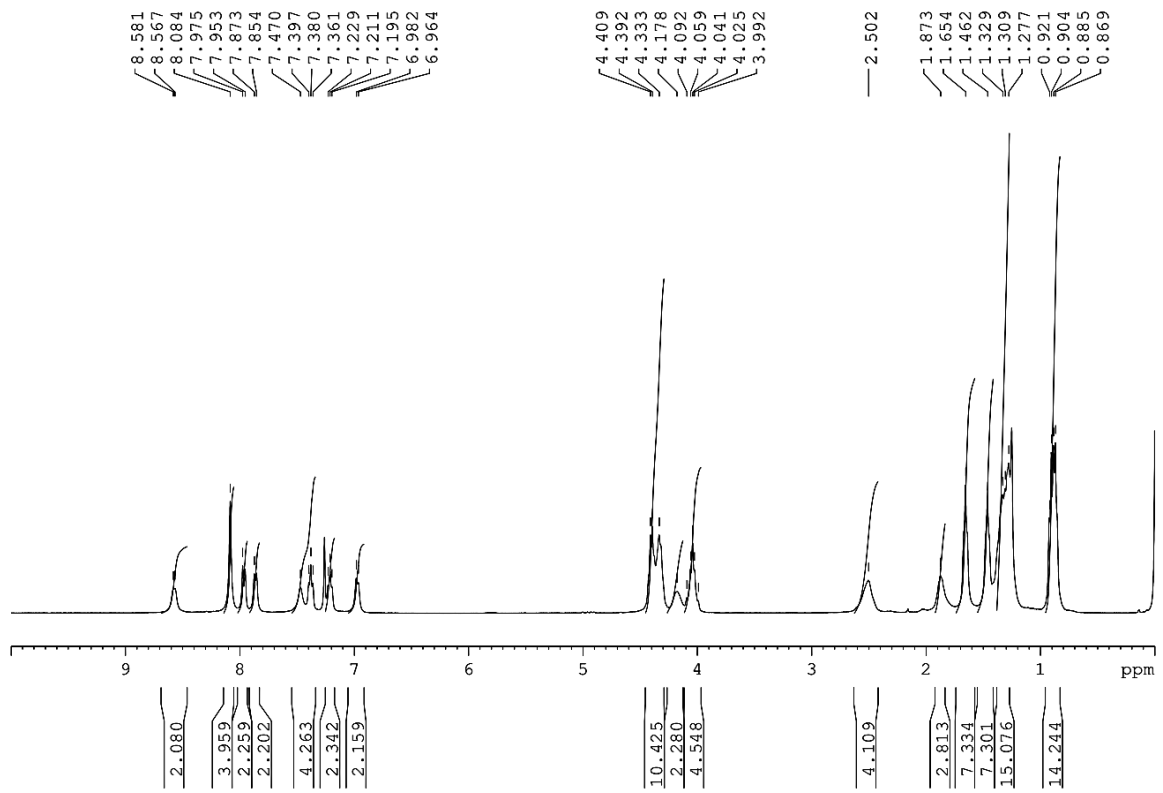

Figure S33. ^{1}H-spectrum of (**S**)-**3** at 25 ºC in $CDCl_3$. (BRUKER AVANCE-400 with 400 MHz)

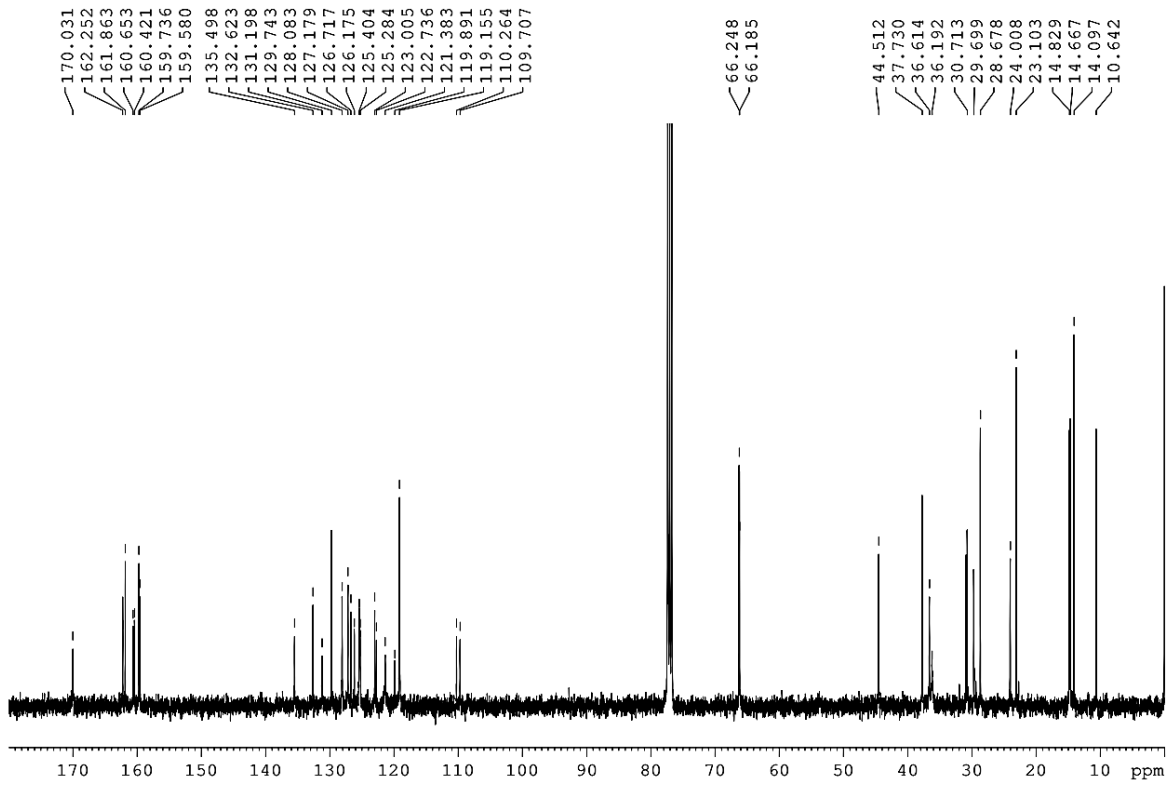

Figure S34. ^{13}C-spectrum of (**S**)-**3** at 25 ºC in $CDCl_3$. (BRUKER AVANCE-400 with 100 MHz)

1.7 References

1. Sarkar, S.; Sarkar, A.; George, S. J., Stereoselective Seed-Induced Living Supramolecular Polymerization. *Angew. Chem. Int. Ed.* **2020,** *59* , 19841-19845.

2. Miros, F. N.; Zhao, Y.; Sargsyan, G.; Pupier, M.; Besnard, C.; Beuchat, C.; Mareda, J.; Sakai, N.; Matile, S., Enolate Stabilization by Anion–π Interactions: Deuterium Exchange in Malonate Dilactones on π-Acidic Surfaces. *Chem. Eur. J.* **2016,** *22*, 2648-2657.

3. Berezin, A. A.; Sciutto, A.; Demitri, N.; Bonifazi, D., Rational Synthesis of AB-Type N-Substituted Core-Functionalized Naphthalene Diimides (cNDIs). *Org. Lett.* **2015,** *17*, 1870-1873.

4. ten Eikelder, H. M. M.; Markvoort, A. J.; de Greef, T. F. A.; Hilbers, P. A. J., An Equilibrium Model for Chiral Amplification in Supramolecular Polymers. *J. Phys. Chem. B* **2012,** *116*, 5291-5301.

5. Meisl, G.; Kirkegaard, J. B.; Arosio, P.; Michaels, T. C. T.; Vendruscolo, M.; Dobson, C. M.; Linse, S.; Knowles, T. P. J., Molecular mechanisms of protein aggregation from global fitting of kinetic models. *Nat. Proto.* **2016,** *11*, 252-272.

6. Narayan, B.; Bejagam, K. K.; Balasubramanian, S.; George, S. J., Autoresolution of Segregated and Mixed p-n Stacks by Stereoselective Supramolecular Polymerization in Solution. *Angew. Chem. Int. Ed.* **2015,** *54*, 13053-13057.

7. Sarkar, S.; Narayan, B.; George, S. J., Circularly Polarized Luminescence from Bischromophoric Cyanostilbene-Derived Homochiral Nanostructures in Solution. *ChemNanoMat* **2020,** *6* (8), 1169-1174.

8. Bentea, L.; Watzky, M. A.; Finke, R. G., Sigmoidal Nucleation and Growth Curves Across Nature Fit by the Finke–Watzky Model of Slow Continuous Nucleation and Autocatalytic Growth: Explicit Formulas for the Lag and Growth Times Plus Other Key Insights. *The Journal of Physical Chemistry C* **2017,** *121* (9), 5302-5312.